Technische Universität Ilmenau
Institut für Mathematik

Preprint No. M **15/01**

Quasistatic inflation processes within compliant tubes : Part 2

Werner Vogt, Joachim Steigenberger, Peter Maisser

Januar 2015

Impressum:
Hrsg.: Leiter des Instituts für Mathematik
Weimarer Straße 25
98693 Ilmenau
Tel.: +49 3677 69-3621
Fax: +49 3677 69-3270
http://www.tu-ilmenau.de/math/

ilmedia

Quasistatic inflation processes within compliant tubes

Part 2: Numerical simulations

Werner Vogt, Joachim Steigenberger, Peter Maisser

January 15, 2015

Abstract

In former work [7], [8], and [9], a mechanical system was considered that models a segment of a live or artificial worm or a balloon for angioplasty that is placed within a cylindrical rigid or compliant tube (vein). Based on the Principle of Minimal Potential Energy and treated as an optimal control problem with state constraint the authors derived a system of differential equations that describes the statics of the inflation process including the shape of the inflated system and the contact forces between balloon and vein. This Part 2 of [8] now presents corresponding simulation results. A short but complete introduction to the theory makes the paper selfconsistent.

Key words Biomechanics, optimal control, state constraint, numerical methods.
MSC 2010 49J15, 49N90, 65L10, 74F10, 74K15.

Contents

1 Introduction

In this paper we continue investigations published in [7],[8],and [9]. There, the authors firstly considered quasistatic ballooning processes of originally cylindrical compliant "segments" - by means of internal pressure expanding either freely or within a rigid tube. In [9], the rigid tube has been replaced with a compliant one. An ODE boundary value problem allows to describe the shape of the system under internal pressure and additional external longitudinal force, and the contact pressure between segment and tube as well. These theoretical investigations were done with a background from mechanics and medicine: peristaltic locomotion of segmented worms used for exploration in hazardous terrain and in minimally invasive surgery. Caused by certain circumstances, the announced simulation results had to be postponed and are now presented in the following.

To make the paper in hand self-contained, we sketch the theoretical results of the foregoing paper. For this end, the paper is organized as follows. Sections 2 and 3 present the physical and the mathematical model of the system to be analyzed. The corresponding essentials are sketched in Figure 1. Section 3 ends up in describing the final boundary value problem, its origin, and its handling. The numerical exploitation of the BVP is explained in Section 4, whereas Section 5 presents simulation results concerning the system behavior under change of relevant parameters. The Conclusion gives a quick summary of what has been done, hints at some facts that might be seen as inadequate to practical applications, and offers corresponding possible improvements.

Some of the improvements (which are to cover wider regions of applications) require slight enlargements of the theory, some can be accomplished simply by interchanging parameter values for others. Any interested specialist is invited to use our source code - on request via the secretary of the Institute of Mathematics (see top).

2 The physical model

A "segment" is a compliant mechanical element that has a hull consisting of two rigid circular discs of radius $r_1 \geq 0$ connected by a deformable membrane of circular cylindrical original shape. The segment is positioned within a compliant circular cylindrical tube ("vein") of radius $r_2 \geq r_1$. Filling the segment with an incompressible fluid the internal pressure makes the segment radially expand - possibly freely at the beginning, then after a first touch together with the vein (a modest scenario of vessel dilation in medical surgery, see [11]). Keeping some working pressure p_0 fixed, two opposite longitudinal forces $\pm f_1$ acting at the discs may press or pull the segment, thereby changing its radial expansion. These forces can be seen as external forces caused by a fluid filling of the tube or as internal ones caused by displacing the segment discs via some mechanical device to be operated from outside.

We emphasize that the following propositions and simulation results do not depend on any geometrical assumptions concerning the shape of the deformed system (as done, e.g., in [2] and [6]). Rather, they are based on clear physical hypotheses and come up by strict mathematical reasoning, see [9].

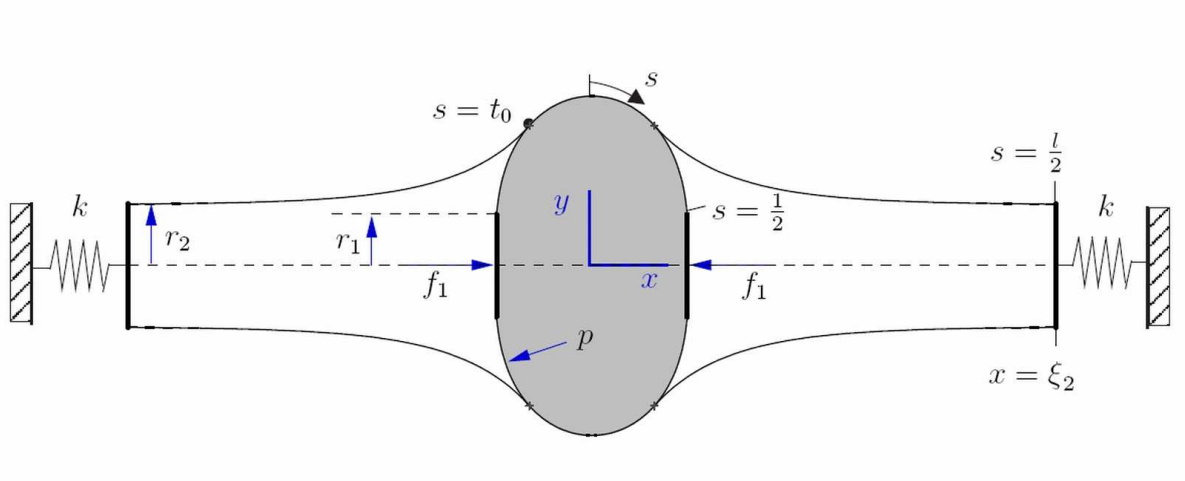

Figure 1: Inflated segment within vein

2.1 Geometric assumptions

(1) The arrangement of the cylindrical parts of the system is of both longitudinal and latitudinal *symmetry* (segment in mid position).

2.2 Physical assumptions

(1) Both vein and (hull of) segment are *membranes* (in the sense of shell theory: zero bending stiffness) and *skin-like* (stable only under tensile internal stresses).

(2) The membranes are of originally *constant thicknesses* h_1 (segment) and h_2 (vein).

(3) The membranes are *meridionally inextensible* and *latitudinally hyper-elastic*. So, the arc-lengths of the meridians are invariant under deformation; hyper-elasticity means stress-strain relations of the form $\sigma = E\chi(\varepsilon)$. For Hooke material we have $\chi(\varepsilon) = \varepsilon$ with given Young's modulus E, else $\chi(\cdot)$ is some smooth function $\mathbb{R}^+ \to \mathbb{R}^+$ with $\chi(0) = 0$ and some suitably chosen fictitious E. The relation of the latitudinal tensile stiffnesses is marked $\beta := h_2E_2/h_1E_1$ ($\beta > 1(< 1)$: "thick(thin)-walled vein").

(4) The supposed meridional inextensibility of the vein excludes any longitudinal fixation of the vein's ends. In order to mimic a real elastic shortening under radial expansion, the ends are to be fastened by means of two elastic springs of stiffness k [1]. The end radii r_2 shall be fixed under deformation (rigid rings).

(5) Any inflation process is to run as slow as to allow to neglect dynamical effects (quasistatic process).

[1] In calculations, k can be chosen arbitrary but positive. $k = 0$ would entail a trivial configuration: stress-free outer parts of the vein with constant radius r_2 and running into the inflated segment with a fold. A closer relation to a longitudinally extensible vein can be achieved by $k = \beta r_2/l$ (stiffness of an extensible cylinder following a Hooke law).

3 The mathematical model

Based on the foregoing working hypotheses the mathematical model was established in [9] by exploiting the Principle of Minimal Potential Energy. The potential energy of the system is an additive composite of (a) the potential energy stored in the deformed membranes, (b) the energy of the inflating fluid, (c) the energy of the longitudinal forces $\pm f_1$, (d) the energy of the elastic springs at the vein ends.

3.1 About notation

(1) In order to get all expressions rid of misplaced ballast (and simultaneously make the model match real systems of any dimension) the following *normalization* is used:

lengths: unit of measure:=L_1=original length of segment
(then, formally, length of segment=1, length of vein=$l > 1$),

pressure: $P = (\frac{2h_1E_1}{L_1})p$,

force: $F = (2\pi h_1 E_1 L_1)f$.

Sometimes it is comfortable to use $q := \frac{1}{p}$ instead of the pressure p.

(2) Due to symmetry the membrane shapes are well-described by the normal equations of the meridians: $\frac{dx}{ds} = \cos(u)$, $\frac{dy}{ds} = \sin(u)$, $\frac{du}{ds} = \varkappa$,
(s: arc-length, x, y: longitudinal and radial coordinate, u: slope, $\varkappa$: curvature, to be found.)

(3) Latitudinal strains and stresses (everything to be labeled 1 or 2):

$\varepsilon(s) = (y(s) - r)/r$, $\sigma(s) = E\chi(\varepsilon(s))$;

let $\psi(y) := \chi(\frac{y}{r} - 1)$, $\Psi(y) := \int_r^y \psi(\eta)d\eta$.

For Hooke material we have $\psi_1(y_1) = \frac{1}{r_1}(y_1 - 1)$, $\psi_2(y_2) = \frac{\beta}{r_2}(y_2 - 1)$.

3.2 The final boundary value problem

(1) Primarily, minimizing the potential energy is a variational problem for the radii y_1, y_2. Considering remark 3.1(2), it can be turned into an optimal control problem with state constraint (y_1 no bigger than y_2) for the slopes u_1, u_2 as controls. In respect of the membrane properties (which allow edges) the slopes are supposed to be piecewise continuous functions with values in $(-\frac{\pi}{2}, \frac{\pi}{2})$, i.e., meridians are piecewise smooth curves, schlicht over the $x-$axis.

(2) A careful analysis of the optimality conditions exhibits the slopes $u_1(s)$, $u_2(s)$ as continuous functions, piecewise smooth (off the junction points, see below) of a smoothness class implied by those of the two elasticity functions χ_1 and χ_2.

(3) The ultimate representation of the mathematical model is the following *parameter-dependent boundary value problem*:

$$\begin{array}{llll} \dot{x} = \cos u, & \dot{y} = \sin u, & \dot{u} = F_0(u, y; p, f_1, \xi_2), & s \in (t_0, 0], \\ \dot{x}_1 = \cos u_1, & \dot{y}_1 = \sin u_1, & \dot{u}_1 = F_1(u_1, y_1; p, f_1), & s \in (-\frac{1}{2}, t_0), \\ \dot{x}_2 = \cos u_2, & \dot{y}_2 = \sin u_2, & \dot{u}_2 = F_2(u_2, y_2; p, k, \xi_2), & s \in (-\frac{l}{2}, t_0), \end{array} \qquad (1)$$

where the right-hand-sides are

$$\begin{aligned} F_0(u,y;p,f_1,\xi_2) &= \{-2py+\psi(y)\cos(u)\}\cos(u)/[py^2-f_1+k\cdot(\tfrac{l}{2}-\xi_2)], \\ F_1(u_1,y_1;p,f_1) &= \{-2py_1+\psi_1(y_1)\cos(u_1)\}\cos(u_1)/[py_1^2-f_1], \\ F_2(u_2,y_2;p,k,\xi_2) &= \psi_2(y_2)\cos^2(u_2)/[k\cdot(\tfrac{l}{2}-\xi_2)]. \end{aligned} \tag{2}$$

The total problem splits into three: one on $(-\frac{l}{2},t_0)$ for the free part of the vein, one on $(-\frac{1}{2},t_0)$ for the free part of the segment, and one on $(t_0,0]$ for that part where segment and vein are in contact ($u_1=u_2=:u$, $y_1=y_2=:y$, $\psi:=\psi_1+\psi_2$ mirror the common deformation of both membranes). All this describes the left half of the system, due to symmetry, the right half comes up simply by reflection with respect to $x=0$. The respective state functions are (u_2,y_2): slope and radius of free vein part; (u_1,y_1): slope and radius of free segment part; (u,y): common slope and radius of vein and segment in contact.

The supplementing *boundary conditions* (prescribing boundary values or continuity, resp.) are the following:

$$\begin{aligned} &y_1(-\tfrac{1}{2})=r_1, \\ &y_2(-\tfrac{l}{2})=r_2, \quad x_2(-\tfrac{l}{2})=-\xi_2, \\ &u(0)=0, \qquad x(0)=0, \qquad y(0)=:y_0. \\ &u_1(t_0)=u_2(t_0)=u(t_0), \\ &y_1(t_0)=y_2(t_0)=y(t_0), \\ &x_1(t_0)=x_2(t_0)=x(t_0). \end{aligned} \tag{3}$$

Parameters to be matched are the *junction point* $t_0<0$ and the actual coordinate of the left vein end $-\xi_2$, only the latter enters the differential equations. In most problems, the equatorial radius y_0 is simply an outcome of evaluations. Besides these to-be-determined parameters the differential equation is entered by the parameters p, f_1, and k which can be adjusted to appropriate values (whereby $F_1(...)$ shows that $f_1\neq pr_1^2$ has to be obeyed). Thereby the internal pressure p is *not* a state variable (as it was in [7]; here, it has practically to be kept constant by means of a fluid reservoir). The further parameters r_1, r_2, l can also get suitable fixed values which then characterize the system dimensions.

(4) With every solution of the boundary value problem the common geometry of both segment and vein on the contact region is well-known (and so are the functions u, y). The normalized *constraint pressure* z (upon segment inwards, upon vein outwards, $z>0$ on the contact area, $z=0$ else) then follows in two equivalent forms from the membrane equations of shell theory (for separated segment and vein),

$$\begin{aligned} 2yz &= 2py-\psi_1(y)\cos u+\dot{u}[\Psi_1(y)+(pr_1^2-f_1)/\cos(\alpha_1)], \\ -2yz &= -\psi_2(y)\cos u+\dot{u}[\Psi_2(y)+k(\tfrac{l}{2}-\xi_2)/\cos(\alpha_2)]. \end{aligned} \tag{4}$$

Here $\alpha_1=u_1(-\frac{1}{2})$, $\alpha_2=u_2(-\frac{l}{2})$, and $\dot{u}$ is simply $F_0(u,y;p,f_1,\xi_2)$.

(5) Geometrically, the supposed meridional inextensibility guarantees the existence of a shape of maximal volume of the segment (formally approached by $p\to\infty$). This shape can be described by means of elliptic integrals (see [8]) and may be used as a starting object in iteration. For this reason it seems useful to have some corresponding data at hand:

The equatorial radius $\overline{y}_0$, length $\overline{l} := 2 \mid x_1(-\frac{1}{2}) \mid$, and volume $\overline{v}$ of the maximal volume segment are[2]

$$\begin{aligned} \overline{y}_0(r_1) &= 0.3824 + 0.7476r_1 + 0.0502r_1^2 + 0.0130r_1^3, \\ \overline{l}(r_1) &= 0.4555 + 0.9761r_1 - 0.7974r_1^2 + 0.2603r_1^3, \\ \overline{v}(r_1) &= 0.1586 + 0.8048r_1 + 2.3471r_1^2 + 0.3017r_1^3. \end{aligned}$$

The above polynomials are L^2-approximates (with coefficients cut to 4 digits).
At our preferred radius $r_1 = 0.1$ we get the values

$$\overline{y}_0 = 0.4577, \quad \overline{l} = 0.5454, \quad \overline{v} = 0.2629,$$

which shall be met in some of the later diagrams.

4 Methods and softwares used for simulation

4.1 A collocation approach

The problem (1),(2),(3) contains several parameters: there are, first, the system parameters $r_1, r_2, l, k, q = 1/p, \beta, f_1$, to be prescribed under the restrictions

$$0 \le r_1 \le r_2, \;\; 1 < l, \;\; 0 < k, \;\; 0 \le q, \;\; 0 < \beta, \;\; f_1 \ne pr_1^2. \tag{5}$$

(To work with q instead of p is reasonable in particular for large values of p in approximating the maximum volume segment shape). Second, there are free, to-be-matched parameters y_0, t_0, ξ_2 undergoing the restrictions

$$r_1 < y_0 \le \overline{y}_0(r_1), \;\; t_0 < 0, \;\; \xi_2 > 0. \tag{6}$$

There are 9 differential equations, 3 to-be-matched parameters, and 12 conditions at the boundary points $-\frac{l}{2}, -\frac{1}{2}, t_0$. So the problem appears as a multi-point boundary value problem with one free boundary t_0. Any numerical solving procedure must be specially tailored, common numerical software is applicable to subproblems like initial-value problems and systems of nonlinear equations only.
Powerful numerical procedures suppose the following standard form of the boundary value problems:

$$\begin{aligned} &\dot{z} = f(t, z), \;\; g(z(a), z(b)) = 0, \\ &z : [a, b] \to \mathbb{R}^n, \quad f : \mathbb{R} \times \mathbb{R}^n \to \mathbb{R}^n, \quad g : \mathbb{R}^n \times \mathbb{R}^n \to \mathbb{R}^n. \end{aligned} \tag{7}$$

[2] In [8], p.567, there is a misprint in (40), to be removed by means of $\int_0^u \sqrt{\cos v}\, dv = 2E(\sin(u/2), \sqrt{2})$.

To this end our problem (consisting of three parts) can be transformed to a 12-dimensional problem on the interval $[0,1]$ by suitable linear transformations $s \rightsquigarrow \tau$ in each partial problem and adjoining three trivial differential equations for the free parameters.

$$\begin{array}{lllll}
(\mathbf{1}) & s = -t_0\tau + t_0, & z_1(\tau) = u(s), & z_2(\tau) = y(s), & z_3(\tau) = x(s); \\
(\mathbf{2}) & s = (t_0 + \frac{1}{2})\tau - \frac{1}{2}, & z_4(\tau) = u_1(s), & z_5(\tau) = y_1(s), & z_6(\tau) = x_1(s); \\
(\mathbf{3}) & s = (t_0 + \frac{l}{2})\tau - \frac{l}{2}, & z_7(\tau) = u_2(s), & z_8(\tau) = y_2(s), & z_9(\tau) = x_2(s); \\
(\mathbf{4}) & & z_{10}(\tau) = y_0, & z_{11}(\tau) = t_0, & z_{12}(\tau) = \xi_2.
\end{array} \tag{8}$$

The transformed boundary value problem, now in standard form for $z : \tau \to (z_1(\tau), ..., z_{12}(\tau))$, $\tau \in [0,1]$, reads

$$\begin{array}{ll}
z_1' = -z_{11} G_0(z_1, z_2; q; f_1; z_{12}), & z_1(1) = 0, \\
z_2' = -z_{11} \sin z_1, & z_2(1) - z_{10}(0) = 0, \\
z_3' = -z_{11} \cos z_1, & z_3(1) = 0, \\
z_4' = (z_{11} + \frac{1}{2}) G_1(z_4, z_5; q; f_1), & z_4(1) - z_1(0) = 0, \\
z_5' = (z_{11} + \frac{1}{2}) \sin z_4, & z_5(1) - z_2(0) = 0, \\
z_6' = (z_{11} + \frac{1}{2}) \cos z_4, & z_6(1) - z_3(0) = 0, \\
z_7' = (z_{11} + \frac{l}{2}) G_2(z_7, z_8; z_{12}), & z_7(1) - z_1(0) = 0, \\
z_8' = (z_{11} + \frac{l}{2}) \sin z_7, & z_8(1) - z_2(0) = 0, \\
z_9' = (z_{11} + \frac{l}{2}) \cos z_7, & z_9(1) - z_3(0) = 0, \\
z_{10}' = 0, & z_5(0) - r_1 = 0, \\
z_{11}' = 0, & z_8(0) - r_2 = 0, \\
z_{12}' = 0, & z_9(0) + z_{12}(0) = 0.
\end{array} \tag{9}$$

Here, the functions G_j stand for F_j, $j = 0, 1, 2$, with $p = 1/q$, see (2). The following values for the given parameters,

$$(r_1,\ r_2,\ l,\ k,\ f_1,\ \beta,\ q) \ =\ (0.1,\ 0.12,\ 2,\ 0.06,\ 0,\ 1,\ 0.01)$$

and the far-off constant start approximations $z_i(\tau) = 0.5$, $i = 1, .., 12$, yield a starting solution $z^*(\tau)$, which always admit a continuation with respect to any of the parameters.
MATLAB$^{\mathrm{TM}}$ offers an efficient collocation procedure [1] to solve boundary and eigenvalue problems in standard form (9). The solutions $z_i(\tau)$ are approximated by piecewise polynomials on a given grid. Their unknown coefficients are computed through the condition that all the ODEs have to be fulfilled exactly at the so called collocation points. This approach avoids all insufficiencies which shooting and finite-difference procedures exhibit in this field. Collocation methods can easily be established by using implicit Runge-Kutta methods, where especially Gauss-Legendre, Radau, and Lobatto formulas are preferred because of their good convergence and stability. The collocation code *bvp4c* of MATLAB implements a three-step Lobatto-IIIA formula [1]. It yields the approximate solution of convergence order 4 via grid adaptation and error control within given absolute and relative tolerance *AbsTol* and *RelTol*, respectively.

In our computations, we decided to use the increased error tolerances *AbsTol*=*RelTol*=10^{-6} and 10^{-8} as well. So, by comparison of the numerical results it can be seen that the built-in error estimates guarantee an accuracy of all results with 6 significant digits, [2]. Another guarantee of correct results was achieved through independent simultaneous computing of choice problems by means of the shooting procedure sketched next. This was done by P. Maisser on a TI-Voyage$^{\text{TM}}$-200 computer using the CAS-software Derive$^{\text{TM}}$ 6.

4.2 A shooting approach

In this method the problem (1),(2),(3) is treated as a three-point boundary value problem which is solved by parallel shooting with respect to the three integration domains $[\mathbf{t}_0, 0]$, $[-\frac{1}{2}, \mathbf{t}_0]$, $[-\frac{l}{2}, \mathbf{t}_0]$, each with the unknown boundary point $\mathbf{t}_0$. A standard ODE-solver with step-size control (Runge-Kutta due to the Bogacki-Shampine 3(2)-formula) is used for the initial value problems

$$\begin{aligned}
&\text{ode (1) with} \quad u(0) = 0, \quad y(0) = \mathbf{y}_0, \quad x(0) = 0\ ;\\
&\text{ode (2) with} \quad u_1(-\tfrac{1}{2}) = \mathbf{u}_{1b}, \quad y_1(-\tfrac{1}{2}) = r_1, \quad x_1(-\tfrac{1}{2}) = \mathbf{x}_{1b}\ ;\\
&\text{ode (3) with} \quad u_2(-\tfrac{l}{2}) = \mathbf{u}_{2b}, \quad y_2(-\tfrac{l}{2}) = r_2, \quad x_2(-\tfrac{l}{2}) = \mathbf{x}_{2b}\ ,
\end{aligned}$$

where each fat letter marks an unknown quantity. Then the six transition conditions at the unknown junction point $\mathbf{t}_0$

$$\begin{aligned}
u(t_0) &= u_1(t_0) = u_2(t_0),\\
y(t_0) &= y_1(t_0) = y_2(t_0),\\
x(t_0) &= x_1(t_0) = x_2(t_0).
\end{aligned}$$

define a system of six nonlinear equations

$$\Phi(\boldsymbol{\alpha}_0) = 0 \tag{10}$$

with respect to the six shooting parameters ($\mathbf{c} := k \cdot (\mathbf{x}_{2b} + \frac{l}{2})$)

$$(\mathbf{y}_0, \mathbf{t}_0, \mathbf{c}, \mathbf{u}_{1b}, \mathbf{x}_{1b}, \mathbf{u}_{2b}) =: \boldsymbol{\alpha}_0.$$

The shooting procedure with the ODEs (1),(2),(3) starts at the known boundary points $0, -\frac{1}{2}, -\frac{l}{2}$ in the direction to t_0, while $\Phi(\boldsymbol{\alpha}_0) = 0$ is solved by a damped Newton-iteration scheme where the Jacobian is approximated by forward differences. In each step the damping factor is selected in such a way that monotonous error convergence

$$err(\boldsymbol{\alpha}_0) := norm(\Phi(\boldsymbol{\alpha}_0)) \to 0$$

takes place. The iteration works exclusively on the admissible domain ($\overline{y_0}(r_1)$ is y_0 in the maximal volume shape)

$$\mathbf{B}:\ \{r_2 \le y_0 \le \overline{y}_0(r_1),\ -\frac{1}{2} \le t_0 \le 0,\ c > 0,\ 0 \le u_{1b} \le \frac{\pi}{2},\ -\frac{1}{2} \le x_{1b} \le 0,\ u_{2b} \ge 0\}.$$

The iteration stops if $err(\boldsymbol{\alpha}_0) < \delta$, where δ denotes a given tolerance radius around the junction point t_0.

The first-contact problem ($y_0 = r_2$) is designed as a 2-point boundary value problem for ODE(2) with $t_0 = 0$, so that the former integration strategy can be used.

For a comparison of this *problem-adapted shooting method* with the *general collocation method* we had to choose the same parameter values in both approaches. Table 1 displays some computed values y_0, t_0, ξ_2 of the boundary conditions (3) with $r_1 = r_2 = 0.1, l = 2, q = 0.01$ and $k = \beta r_2/l$, which were obtained by shooting for different β.

β	y_0	t_0	ξ_2
0.01	0.453 959 52	-0.407 048 42	0.809 676 0
0.1	0.453 983 50	-0.407 871 31	0.810 508 80
0.2	0.453 562 57	-0.408 093 40	0.811 152 52
0.4	0.452 933 38	-0.408 517 14	0.811 635 51
0.6	0.452 224 09	-0.409 037 85	0.812 414 04
0.8	0.451 509 09	-0.409 198 95	0.813 072 50
1.0	0.450 785 01	-0.409 812 66	0.813 767 94

Table 1: Results of the shooting approach with tolerance $\delta = 0.002$

β	y_0	t_0	ξ_2
0.01	0.454 311 32	-0.407 496 16	0.810 146 58
0.1	0.453 999 05	-0.407 693 25	0.810 477 98
0.2	0.453 650 55	-0.407 912 66	0.810 847 38
0.4	0.452 948 65	-0.408 352 80	0.811 589 93
0.6	0.452 240 15	-0.408 794 71	0.812 337 51
0.8	0.451 524 95	-0.409 238 40	0.813 090 18
1.0	0.450 802 98	-0.409 683 87	0.813 847 96

Table 2: Results of the collocation approach with tolerance $tol = 10^{-6}$

The corresponding values of the *collocation method* with error tolerances $AbsTol$=$RelTol$=10^{-6} can be seen in Table 2. Obviously these very different approaches yield results which agree by three significant digits. For larger values of parameter β this coincidence is slightly better.[3]

Finally the computations were repeated with increased accuracy $AbsTol$=$RelTol$=10^{-8} of the *collocation code*. But the results rounded to 8 digits are identical with those of Table 2. For a more precise comparison of both accuracies we display some y_0-results and their differences Δ in Table 3. They show that the accuracy $AbsTol$=$RelTol$=10^{-6} will be small enough for all our following computations.

[3]Table 2 and its graphical output were obtained by MATLAB^{TM} on a Toshiba Satellite notebook (2 core, 2.27 GHz) within 8 seconds.

β	$tol = 10^{-6}$	$tol = 10^{-8}$	Δ
0.0	0.454 345 934 202	0.454 345 934 621	$4.19 \cdot 10^{-10}$
0.01	0.454 311 318 439	0.454 311 318 953	$5.14 \cdot 10^{-10}$
0.1	0.453 999 051 984	0.453 999 052 450	$4.66 \cdot 10^{-10}$
1.0	0.450 802 983 342	0.450 802 983 049	$-2.93 \cdot 10^{-10}$

Table 3: Values y_0 of the collocation approach and their difference Δ

5 Simulation results

We emphasize that our simulations do not aim at the investigation of real processes such as, e.g., the active behavior of a worm segment during crawling through a tube, or details in angioplasty (human vessel dilation). Rather, the numerical analysis of our model (that was, indeed, set up in view to such real processes) is to be seen as an instrument to gain insight into the principal behavior of the background paradigm systems. To this end, most of the following simulations were done with fixed system parameters except one or two distinguished ones (e.g., pressure p and vein stiffness β). Through varying the latter, their influence over certain state functions of interest (e.g., segment radius y_0 or constraint pressure z) becomes evident.

In nutshell, the goal of the simulations is to find *general* propositions about the behavior of the modeled systems.

Possibly, the chosen parameter intervals might show some subjective arbitrariness to the specialist. This originates, primarily, in our simplifying use of elasticity moduli which are of considerable uncertainty (in particular those of the multi-layered animal tissues) and nevertheless determine the units of measure used for normalization. We hope not to be too far off the mainstream. As another drawback specialists could see the sole use of Hooke elasticity in the simulations ($\psi(\cdot)$ linear function). It is of no trouble to treat nonlinear hyperelasticity simply by choosing any different nonlinear $\psi-$functions [7]. For our first, principal investigations linearity has been regarded as sufficient.

Doing simulations, we could recognize that certain parameter values did not lead to significant results. So, e.g., large values of the vein length l exhibited a long, nearly undeformed part of the vein during inflation (while wasting computing time). That is, why most calculations were done with $l = 2$. Similarly, preferred values of the radii are $r_1 = 0.1$ and $r_2 = 0.12$. This leads to reasonably tall segment and vein while letting sufficient space for free inflation of the segment until touch with the vein.

5.1 System shape under free and constrained inflation

In order to get a *visual* impression of what happens under increasing pressure p we first choose the system data

- $r_1 = 0.1$ (radius of segment),
- $r_2 = 0.15$, $l = 2$ (radius and length of vein),
- $\beta = 1$ (identical membranes of segment and vein),

- $k = 1$ (substitute for longitudinal vein extensibility),
- $f_1 = 0$ (no extra forces upon segment).
  This last setting $f_1 = 0$ holds for the complete section 5.1.

Then we solve the boundary value problem (9) with several values of $q = 1/p$. The joint

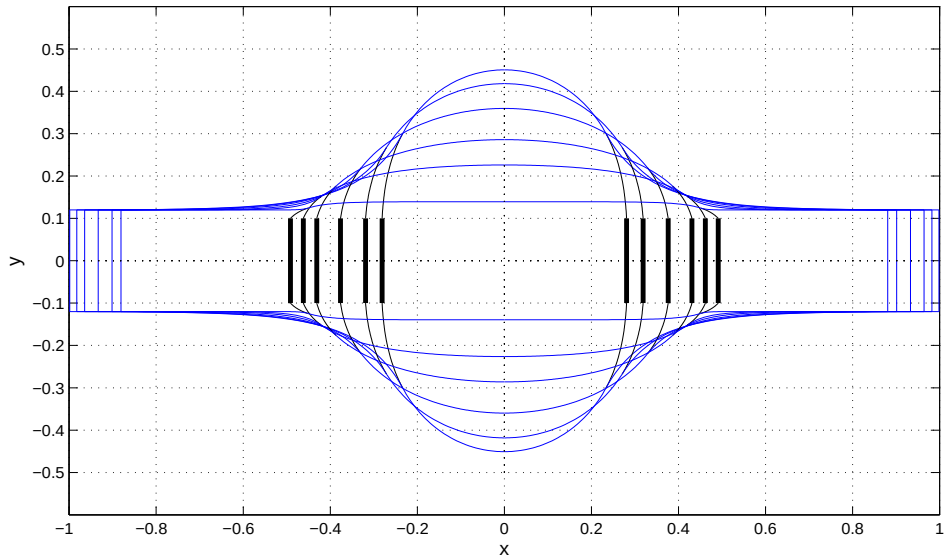

Figure 2: Shapes under pressure $p = 2$, 5, 6.667, 10, 20, 100

graphs of the solutions (z_3, z_2), (z_6, z_5) and (z_9, z_8) - colored blue, and representing the membrane meridians - sketch the left upper part of the system profile (longitudinal cut of the deformed system), the rigid discs are given fat and black. Only Figure 2 shows the total profile (gained through the postulated system symmetry). Later, a 3D image of the complete system is achieved through rotation about the x-axis. Figure 3 is to give a more

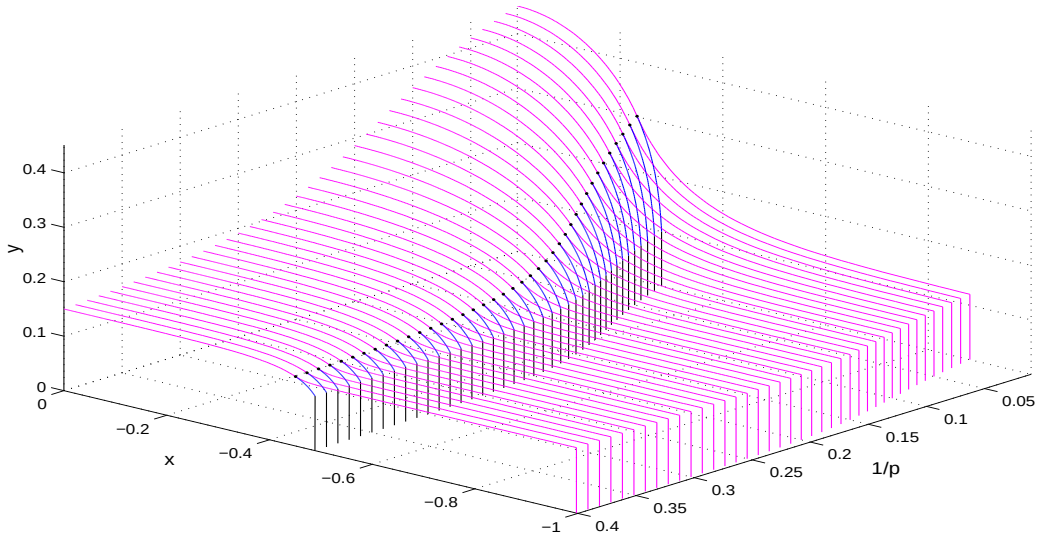

Figure 3: Shapes under various pressures p

vivid impression of how the system deforms under variation of the internal pressure. Each cut parallel to the $x, y-$plane shows the (right upper part of the) profile (mind different scalings of x and y!). The junction points are emphasized.
The first touch occurs at $p \approx 1.67$. The pressure $p = 100$ approximates the fictitious pressure $p = \infty$, that stands for the (theoretically important and β-independent) configuration with a segment of maximal volume.

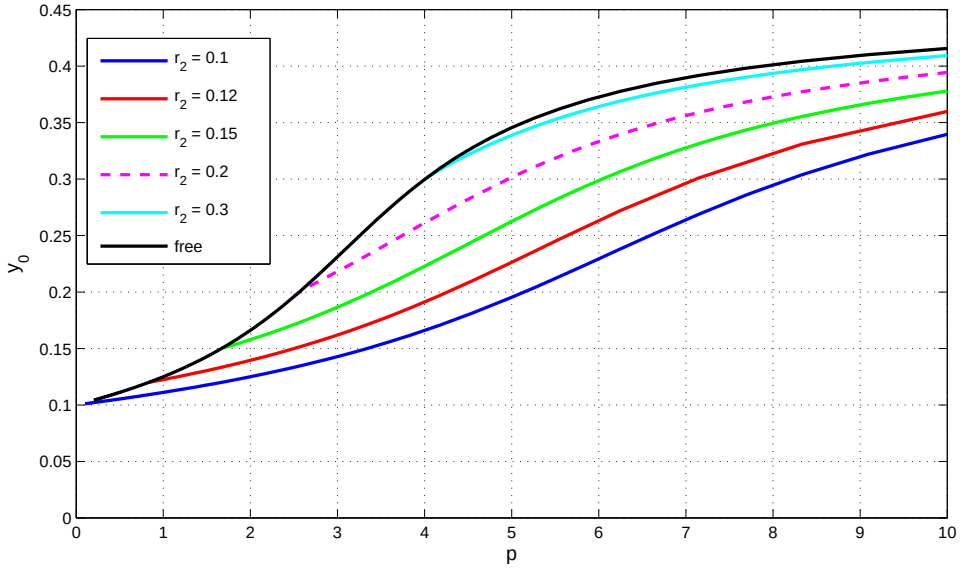

Figure 4: Equatorial radius y_0 vs. pressure p for vein with radii r_2 and $\beta = 1$

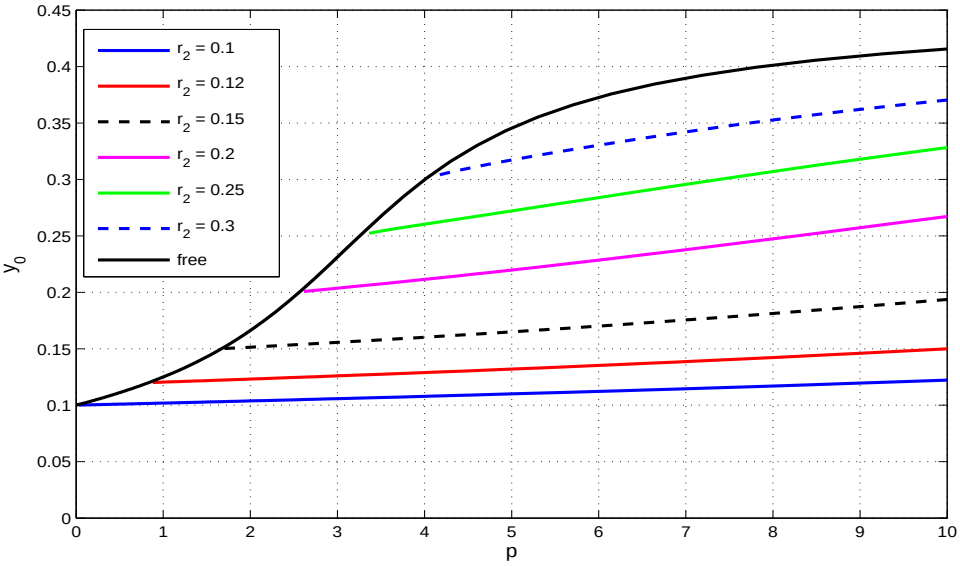

Figure 5: Equatorial radius y_0 vs. pressure p for vein with radii r_2 and $\beta = 10$

Maybe, the actual $y_0 = y_{s=0}$ (equatorial radius) could be seen as the most important quantity during inflation. Figures 4 and 5 show the graphs of $p \to y_0$ for a segment of radius $r_1 = 0.1$ and veins of various radii $r_2 \geq r_1$ with $\beta = 1$ ("thin vein") and $\beta = 10$ ("thick vein"),

respectively. The upper curves represent $p \to y_0$ for free inflation (vein radius $r_2 > \overline{y}_0(r_1)$). The influence of the (thickness or stiffness) parameter β is obvious and might have been expected: the growth of y_0 with p slows down with increasing β because of the increasing resistance of the vein. The limit $\lim_{p\to\infty} y_0$ remains the same for all β. This effect is plausible and can be seen for higher pressure in Figure 6, where every curve asymptotically goes to $\overline{y}_0(0.1) \approx 0.457$ for $p \to \infty$.

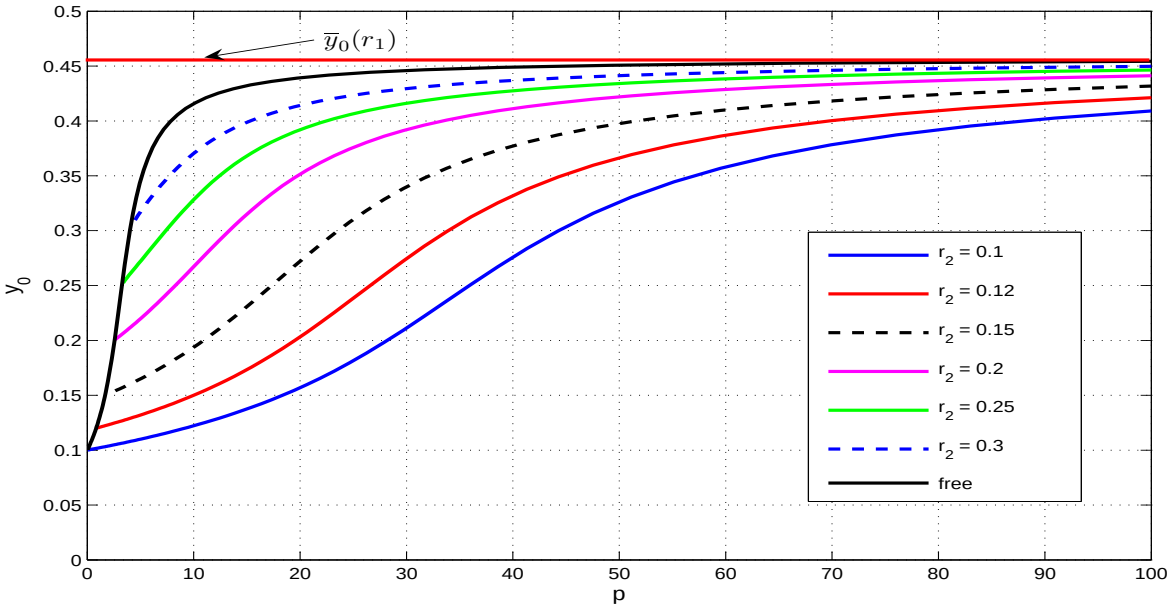

Figure 6: Equatorial radius y_0 vs. pressure $p = 0...100$ for vein with radii r_2 and $\beta = 10$

The transition from free to constrained inflation shows up as a break point of good clearness for large β. Principally, this effect could be used in practice for detecting the event of

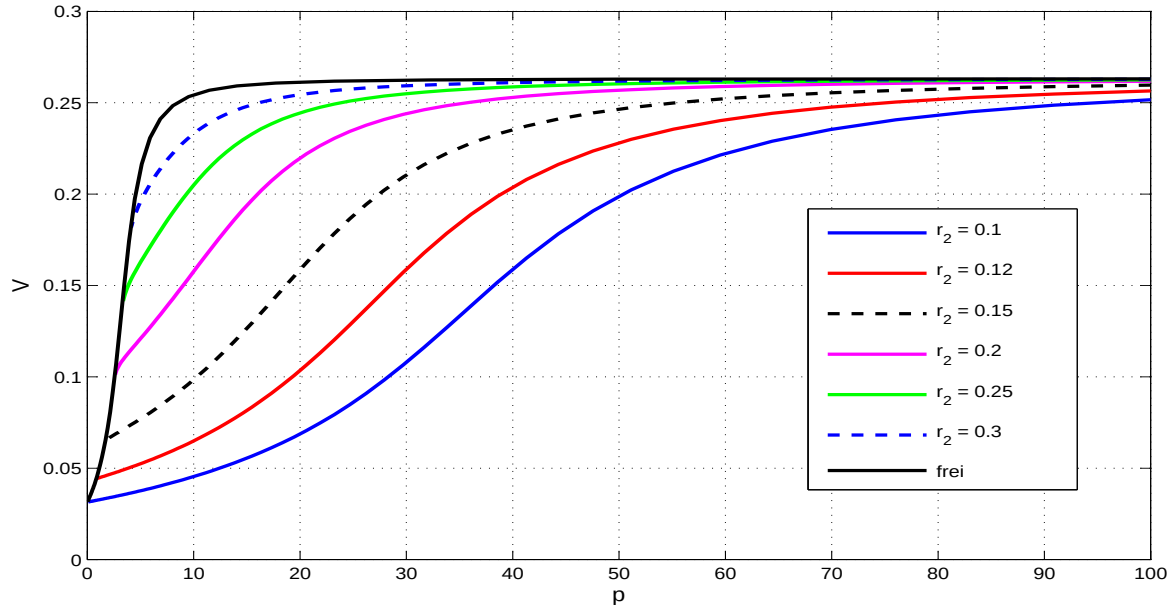

Figure 7: Segment volume v vs. pressure $p = 0...100$ for vein with radii r_2 and $\beta = 10$

first touch segment-vein during inflation (thereby discovering the possibly unknown r_2). Now, since y_0 is, for instance in angioplasty, invisible, one could turn to the observable *segment volume* which, simultaneously with p, can be controlled from outside during filling the segment with fluid. Figure 7 sketches the effects for $\beta = 10$. This figure is the counterpart to Figure 6, it serves for comparison of the effects in observing either y_0 or v.

Figures 8 to 11 sketch the system profiles under various values of the pressure p and the vein stiffness β in different representations. It can be clearly seen how at a fixed working pressure the equatorial radius y_0 of the segment becomes smaller for bigger β whereas the segment length growths.

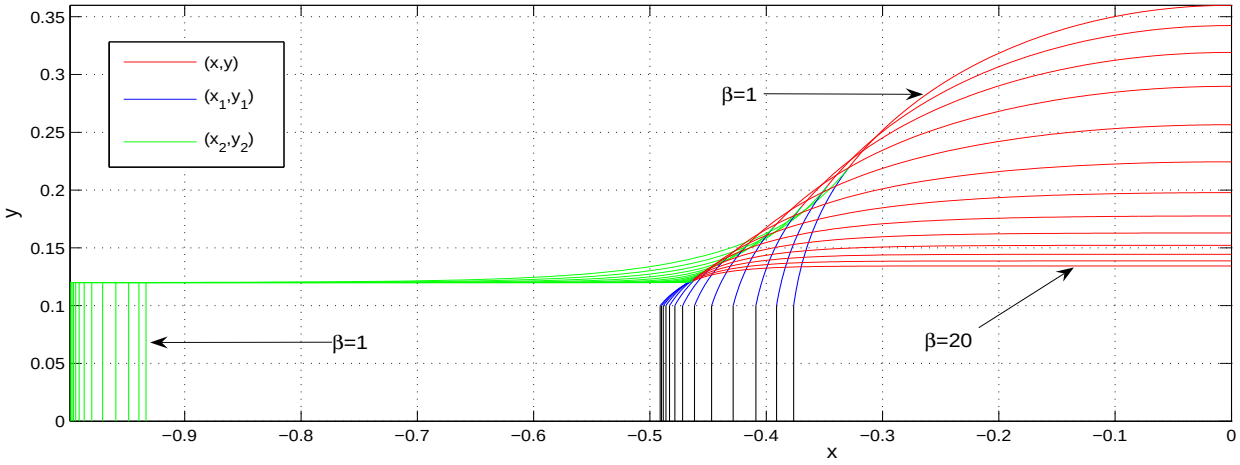

Figure 8: Shapes at $p = 10$, $r_2 = 0.12$ for thickness $\beta = 1 \ldots 20$

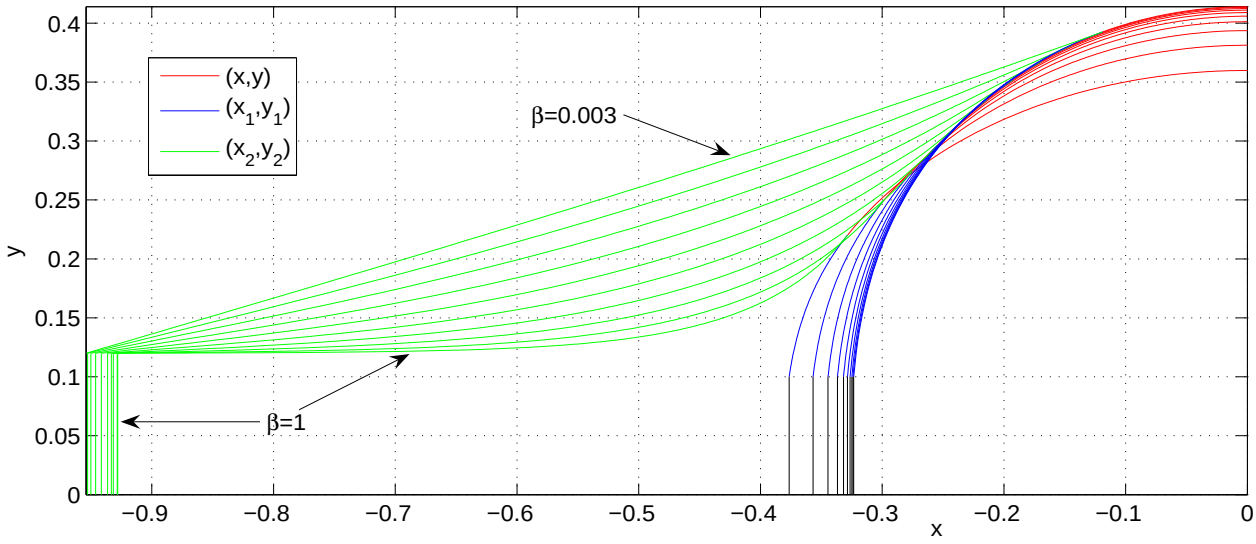

Figure 9: Shapes at $p = 10$, $r_2 = 0.12$ for thickness $\beta = 0.003 \ldots 1$

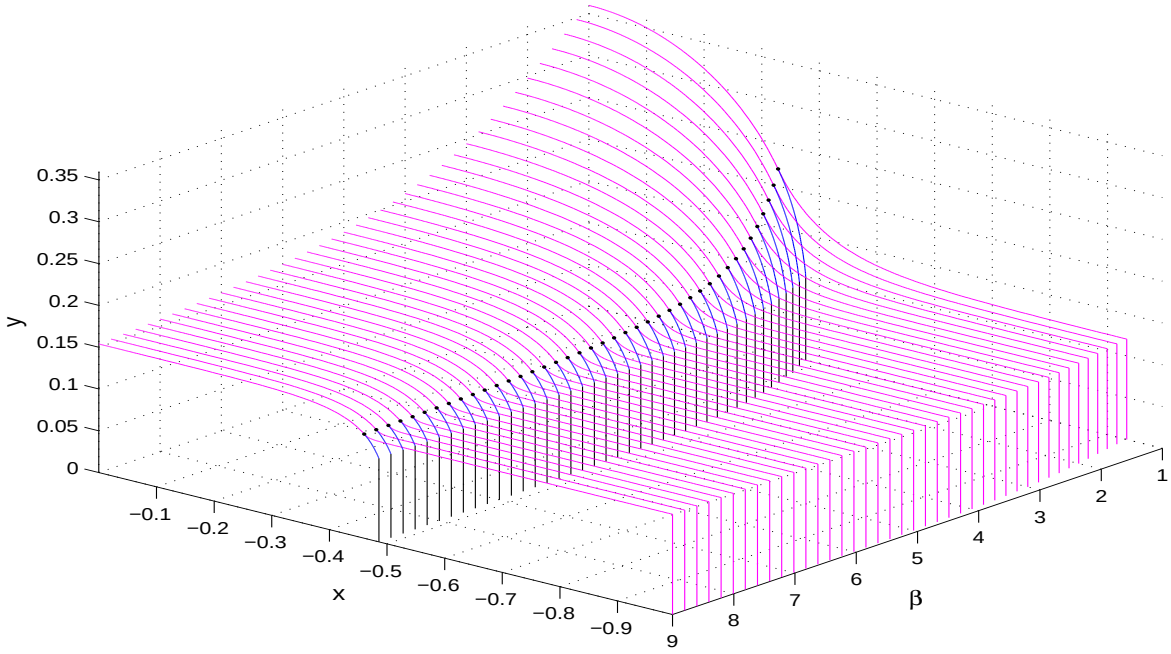

Figure 10: Shapes at $p = 10$, $r_2 = 0.12$ for thickness $\beta = 1 \ldots 9$

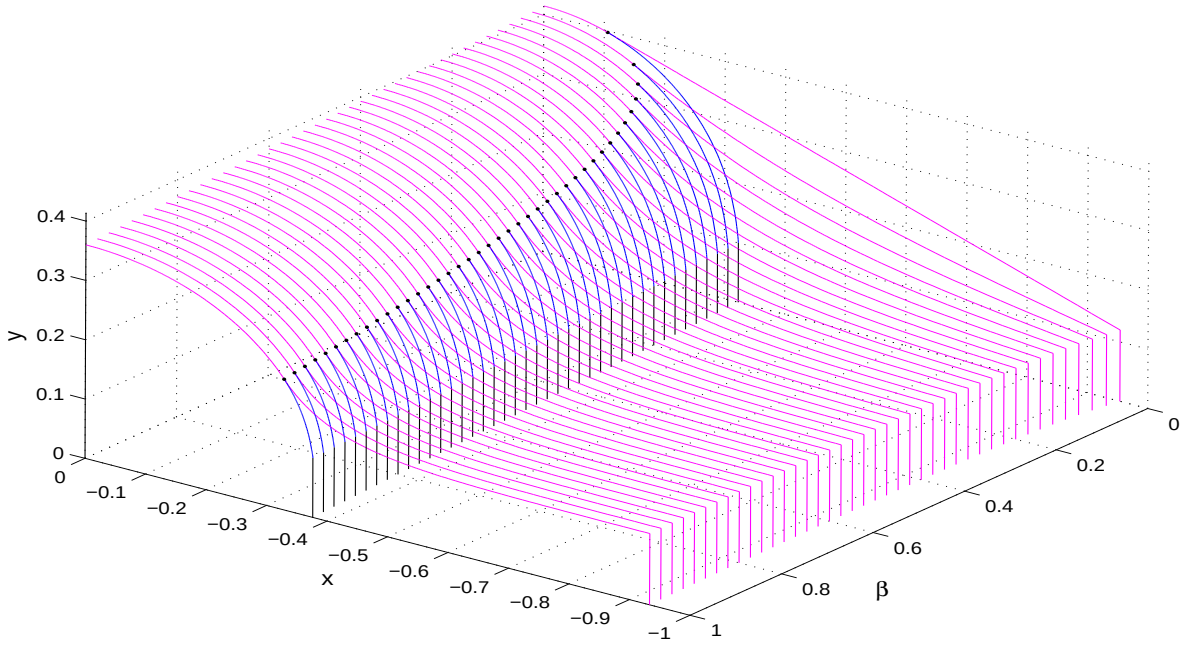

Figure 11: Shapes at $p = 10$, $r_2 = 0.12$ for thickness $\beta = 0.003 \ldots 1$

Figure 12 then shows the effect of p on the system shape during inflation with two different stiffnesses $\beta = 1$ and $\beta = 10$.

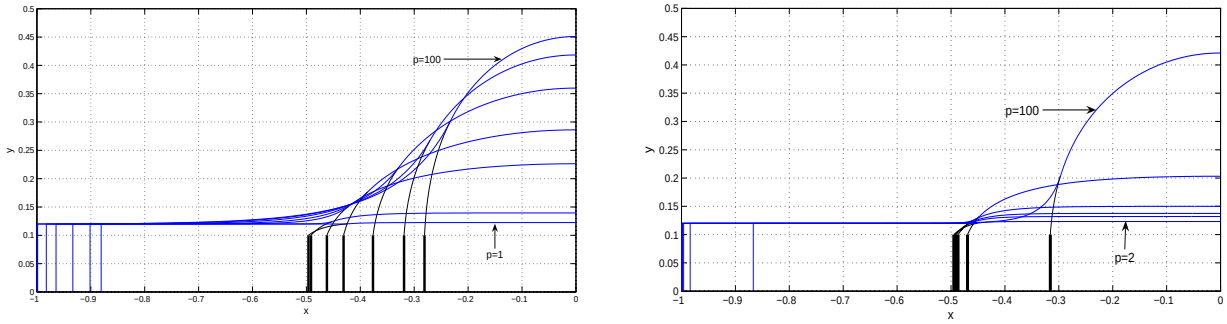

Figure 12: Shapes under pressure $p = 1,\ 2,\ 5,\ 6.667,\ 10,\ 20,\ 100$ for $r_2 = 0.12$ and $\beta = 1$ (left), $\beta = 10$ (right).

For the sake of completion we present the dependence of the segment's length $2 \mid x_1(-\frac{1}{2}) \mid$ on the pressure p in Figure 13. The asymptotic length for $p = \infty$ is $\overline{l} = 0.5454...$

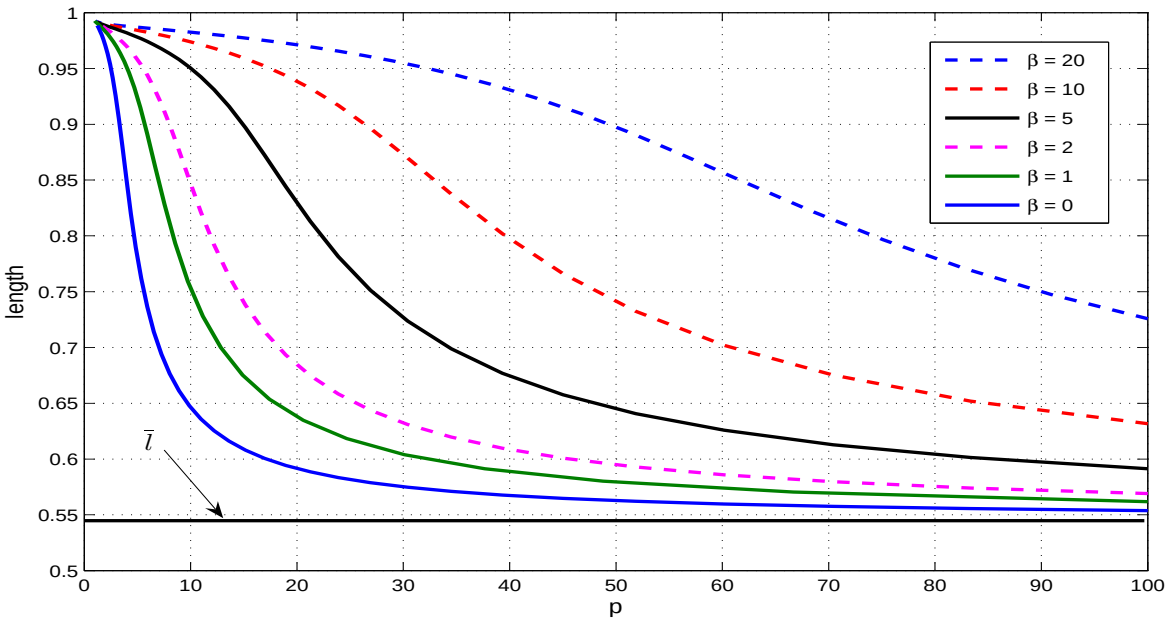

Figure 13: Length of the segment vs. pressure p for various β

5.2 The contact pressure

As we have seen above, the system behavior during inflation, i.e., during filling the segment with fluid, always follows the same line. Suppose $r_2 > r_1$. Then, with $p = 0$ (segment just full of fluid) both segment and vein have their original stress-free cylindrical shape. Increasing p means supply of fluid, the segment shows a radial expansion coupled with a longitudinal shortening, the vein remains undeformed. At a certain p_1 the equatorial radius of the segment equals r_2, that is, there is a point touch of the meridians of segment and vein. Further on, $p > p_1$, segment and vein undergo a joint deformation whereby both membrane meridians coincide along an interval $[t_0, -t_0]$ of the arc-length (t_0 is taken negative in calculating the upper left part of the profile). The points t_0 and $-t_0$ are called *junction points* since outside the interval the meridians of segment and vein separate. This scenario continues (in theory) up to $p = \infty$.

Now, in the inflation phase $p > p_1$ the membranes of segment and vein on a non-void area press against each other. We want to investigate this contact pressure z, its dependence on system parameters and its distribution over the contact area. That the junction point t_0, and so the contact area as well, depend on p and β is already known from the foregoing considerations.

The line of investigation is evident. First, solve the boundary value problem (9) with the preferred parameter values and find, among others, the junction point t_0 and the function $s \mapsto (u, y, x)(s), \quad s \in [t_0, 0]$. Second, introduce these functions into (4) to get the contact pressure z as a function of s and dependent on the parameters.

Figure 14 sketches the distribution of z under various values of p and β. Mind that here the distribution is presented over the longitudinal coordinate x instead of s. Obviously, z has

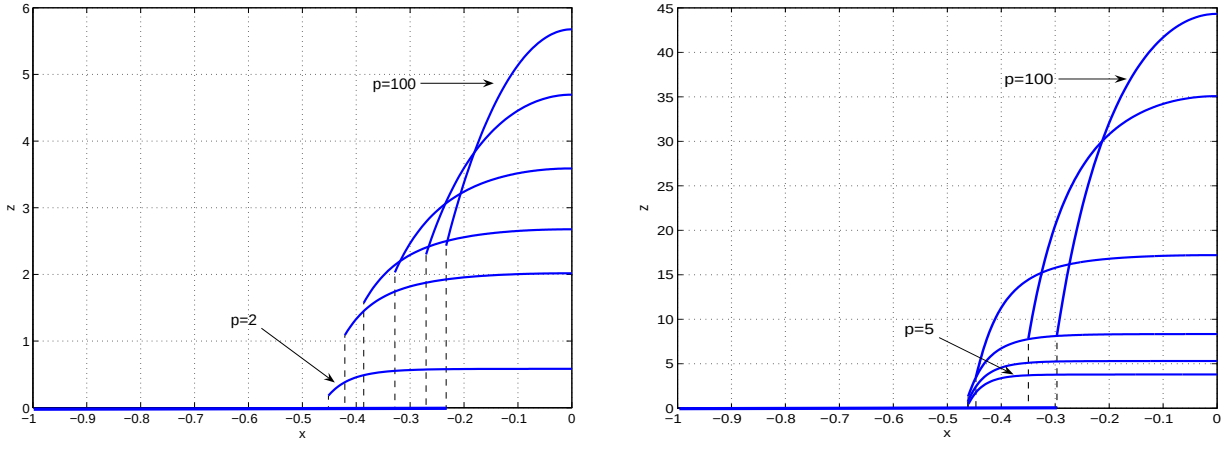

Figure 14: Contact pressure z vs. x for $\beta = 1$ and $p = 2$, 5, 6.667, 10, 20, 100 (left); for $\beta = 10$ and $p = 5$, 6.667, 10, 20, 50, 100 (right).

its maximum at $x = 0$ and jumps down to zero at $x(t_0)$. A 3-dimensional representation is given in Figures 15 and 16. Finally, Figure 17 shows the dependence of the maximum contact pressure $z_0 = z(0, p)$ on p for various β.

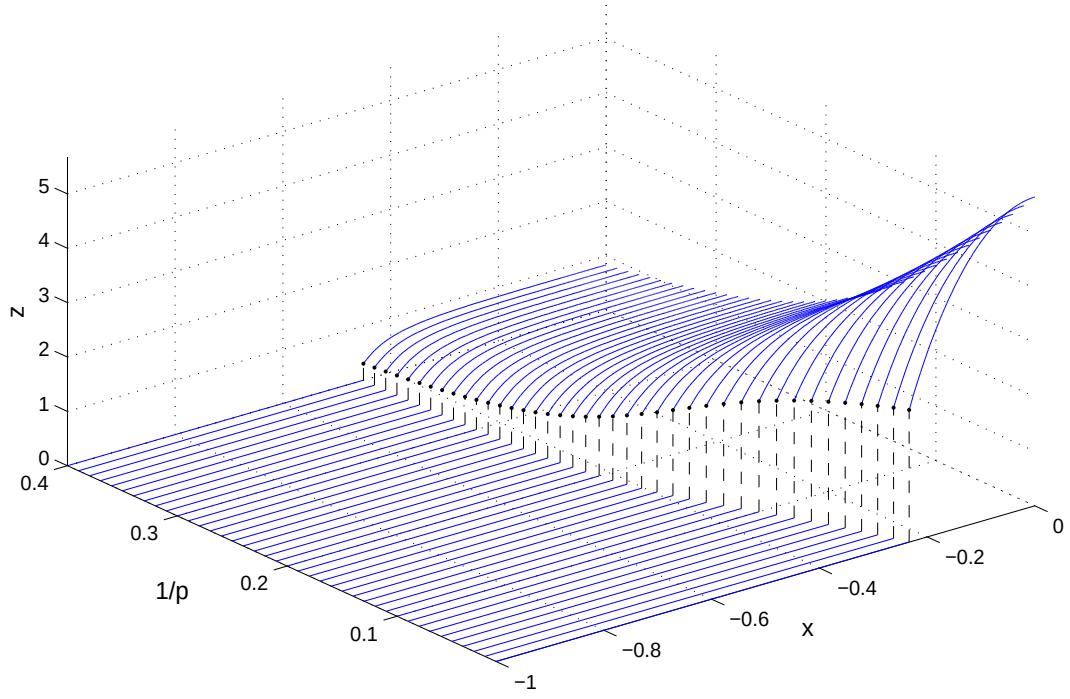

Figure 15: Contact pressure $z(x,p)$ vs. $(x,\frac{1}{p})$ for $\beta = 1$

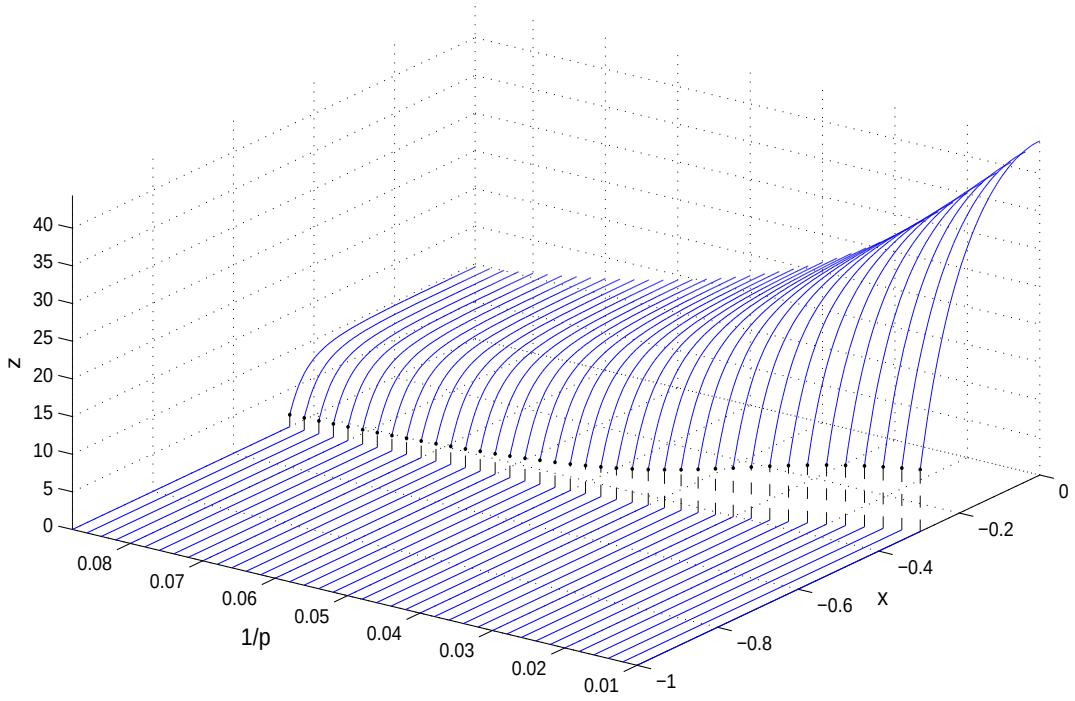

Figure 16: Contact pressure $z(x,p)$ vs. $(x,\frac{1}{p})$ for $\beta = 10$

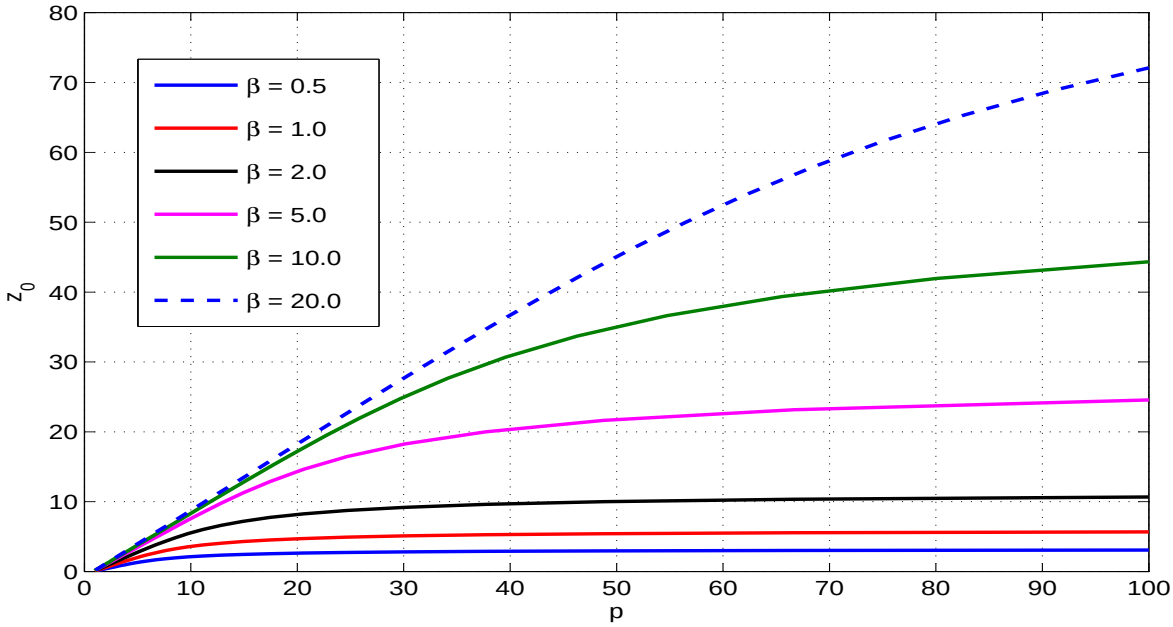

Figure 17: Maximal contact pressure $z_0 = z(0, p)$ vs. p for various β

5.3 Effects of the longitudinal force f_1

Until now, our investigations disregarded the opposite longitudinal forces f_1 which optionally press ($f_1 > 0$) or pull ($f_1 < 0$) at the discs of the segment. These forces have been introduced in order to mimic some (surgical) action in a system state of constant working pressure p_0. The influence of f_1 (at this pressure p_0) on the system can be expected as follows.

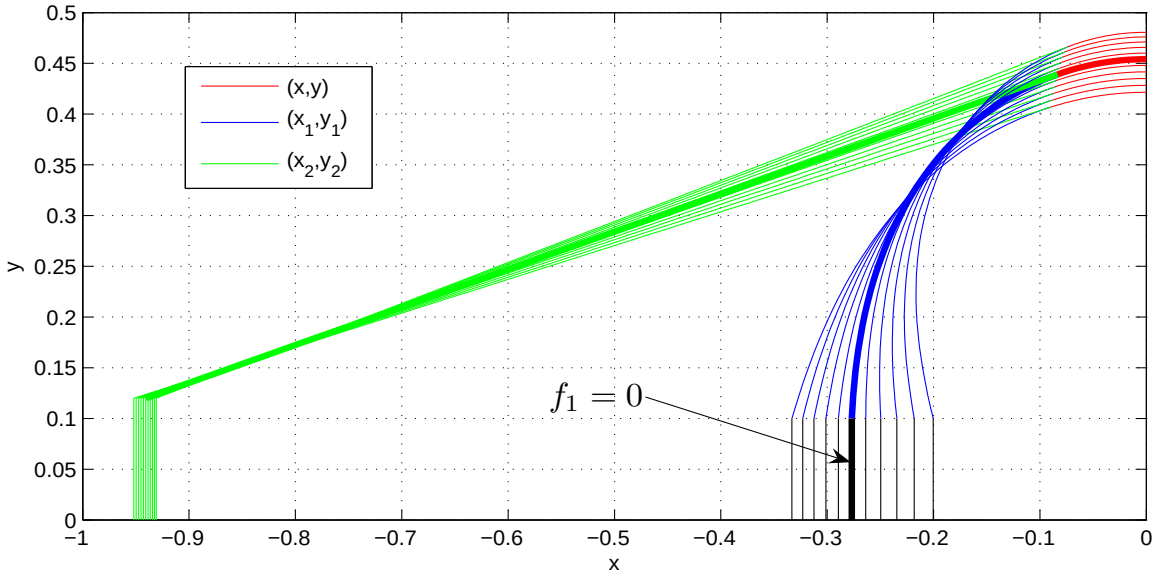

Figure 18: System profiles with $\beta = 0$, $p = 100$, for $-5 \leq f_1 \leq 5$.

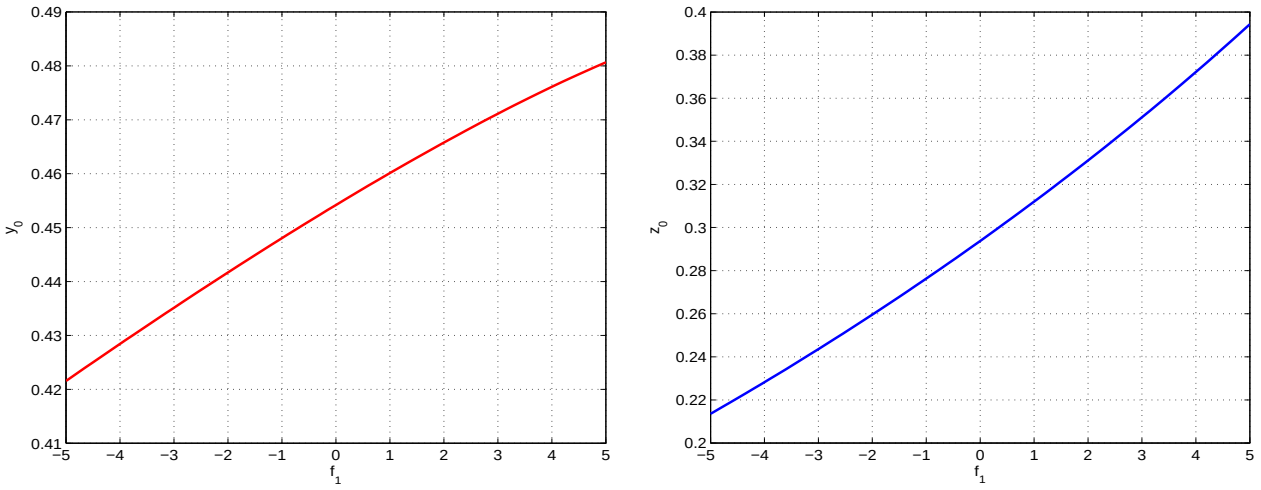

Figure 19: Characteristics from Fig. 18: y_0 vs. f_1 (left), $z_0 = z\,|_{s=0}$ vs. f_1 (right).

Both radius y_0 and length $2 \mid x_1 \mid$ of the segment depend on f_1, that means the segment behaves like a spring (certainly of nonlinear characteristic which will be essentially determined by the parameters p_0 and β). Also the length of the contact interval $2 \mid t_0 \mid$ and the contact pressure z shall vary with f_1 and oscillate about their steady values at p_0 if f_1 repeatedly changes its sign.

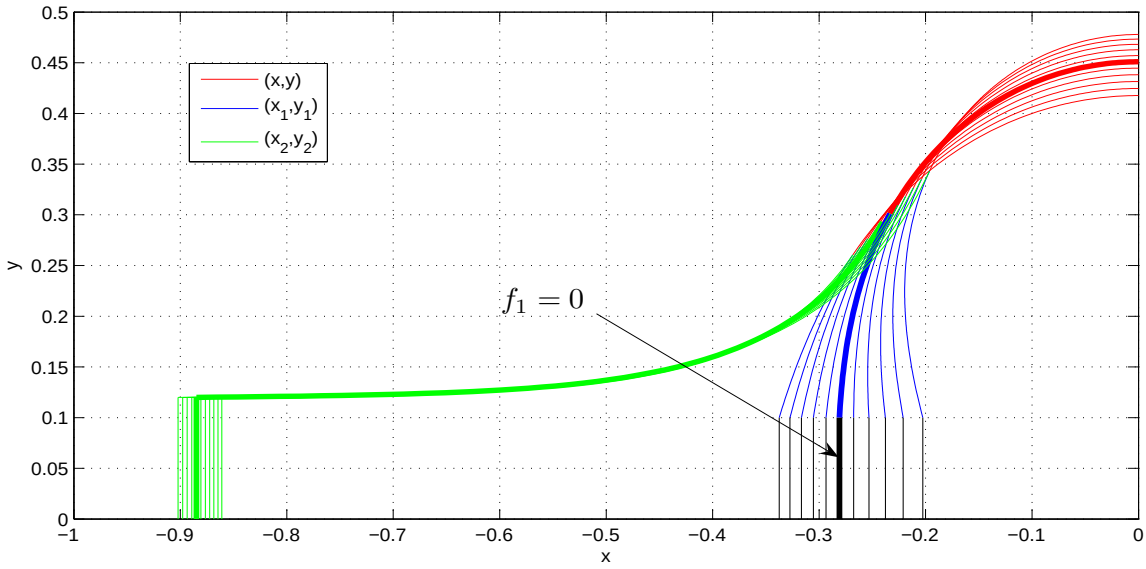

Figure 20: System profiles with $\beta = 1,\ p = 100$, for $-5 \le f_1 \le 5$.

The following figures (numerical results gained by exploitation of (9)) are to give an impression of these dependencies. Mind that (2) gives a hint to precaution: f_1 should be unequal to pr_1^2 (denominator of F_1!). For small pressing $f_1 < pr_1^2$, the segment profile is convex, whereas it becomes tyre-like for $f_1 > pr_1^2$ ($\alpha_1 > \frac{\pi}{2}$). (See [7], where this singularity is overcome by a suitable transformation.)

We start with systems of high internal pressure $p = 100$ and vein stiffness $\beta = 0$. This is a "hard" segment and a "ghost vein", i.e. a meridianally inextensible and of zero circumferential tension (stiffness $E_2 h_2 = 0$). First, we show the change of system shape under the action of pulling or pushing f_1 in Figure 18.

Figure 19 sketches the corresponding behavior of two important state functions: equatorial radius y_0 and maximal contact pressure $z_0 = z$ at $s = 0$.

Effects of greater vein stiffness become clear in Figures 20, 21 and 22 showing system shapes and characteristics as before.

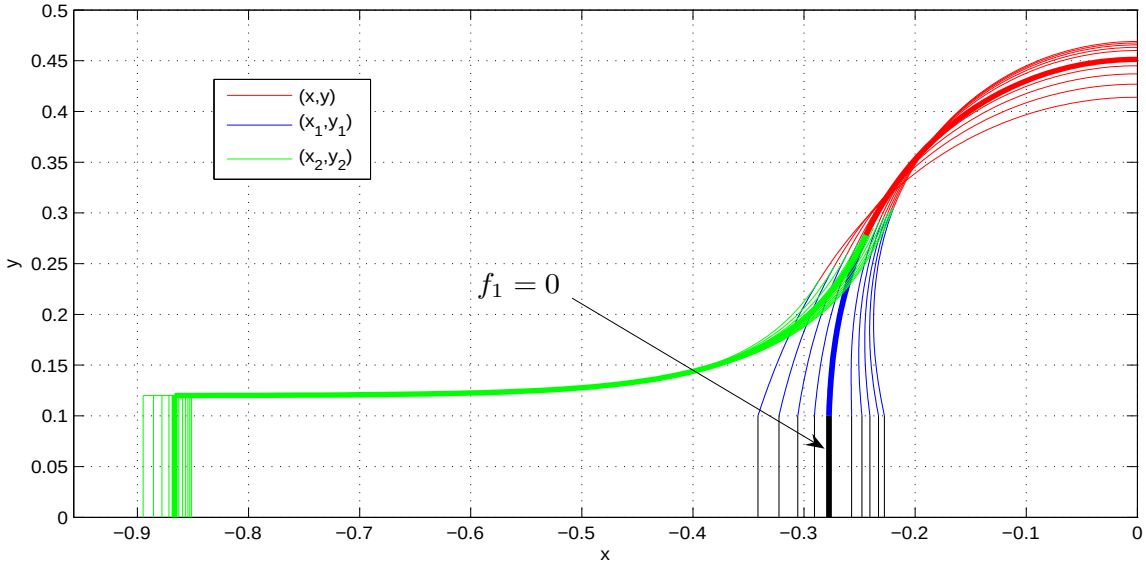

Figure 21: System profiles with $\beta = 2$, $p = 100$, for $-5 \leq f_1 \leq 3.66$.

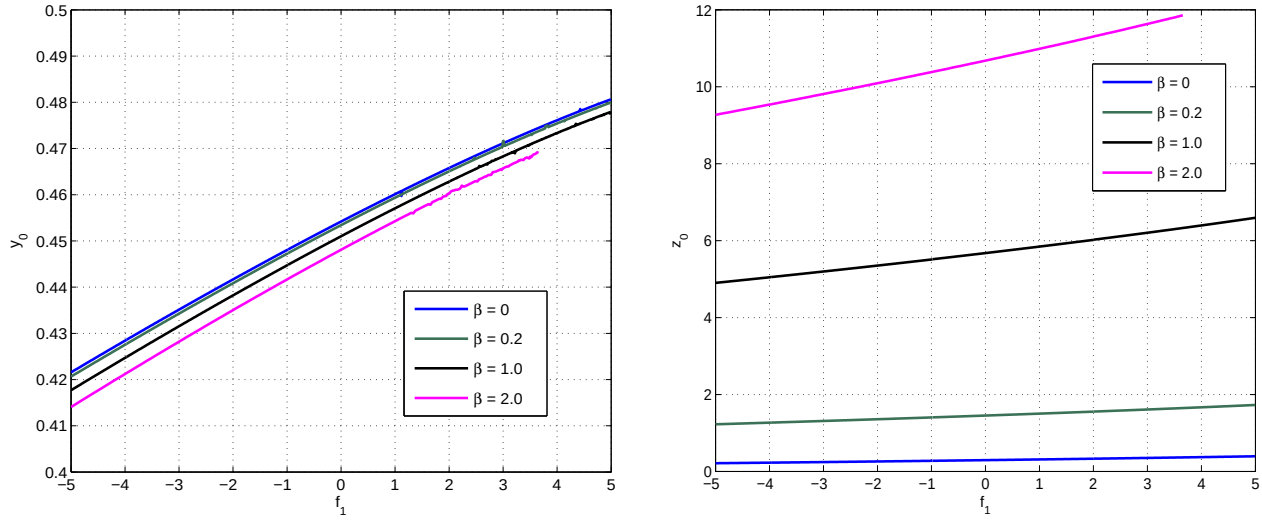

Figure 22: y_0 vs. f_1 (left), $z_0 = z\,|_{s=0}$ vs. f_1 (right) for various β.

The non-straight vein profile for $\beta > 0$ is due to the fact that now the circumferential tension in the vein, $E_2h_2 = \beta E_1h_1$, is not zero anymore. A vein with $\beta = 0$ stands for an extremely thin vein (which is, nevertheless, longitudinally inextensible). So its effects on shape and contact pressure mainly come from the end springs of stiffness k which are to mimic some longitudinal extensibility. The influence of k in this case and for comparison in the case $\beta = 1$ is demonstrated in Figures 23 and 24.

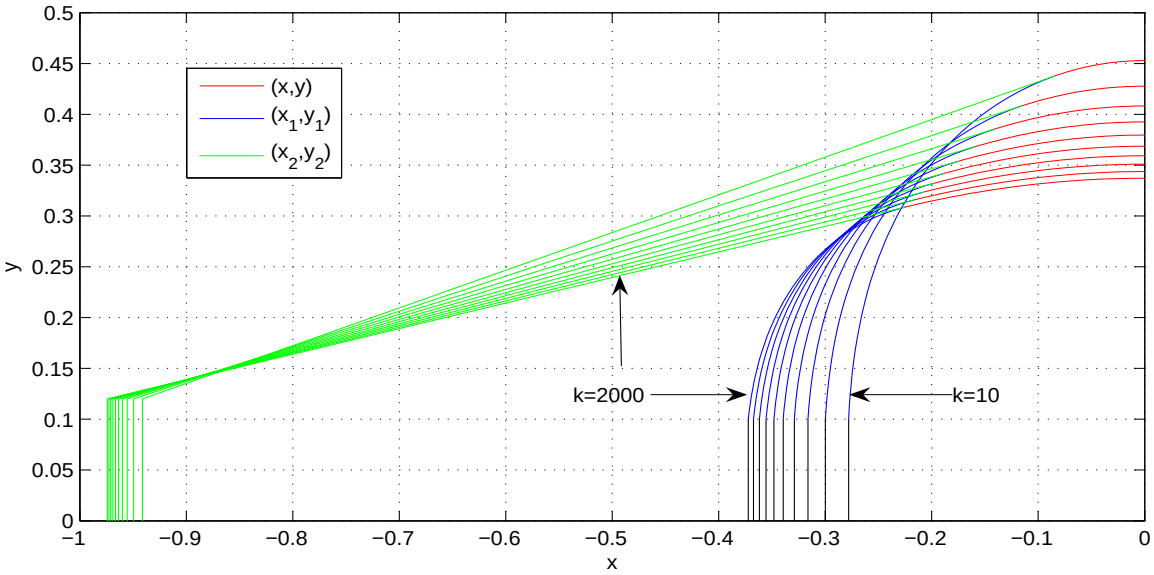

Figure 23: System profiles with $\beta = 0,\ p = 100,\ f_1 = 0$ with $k = 10 \ldots 2000$.

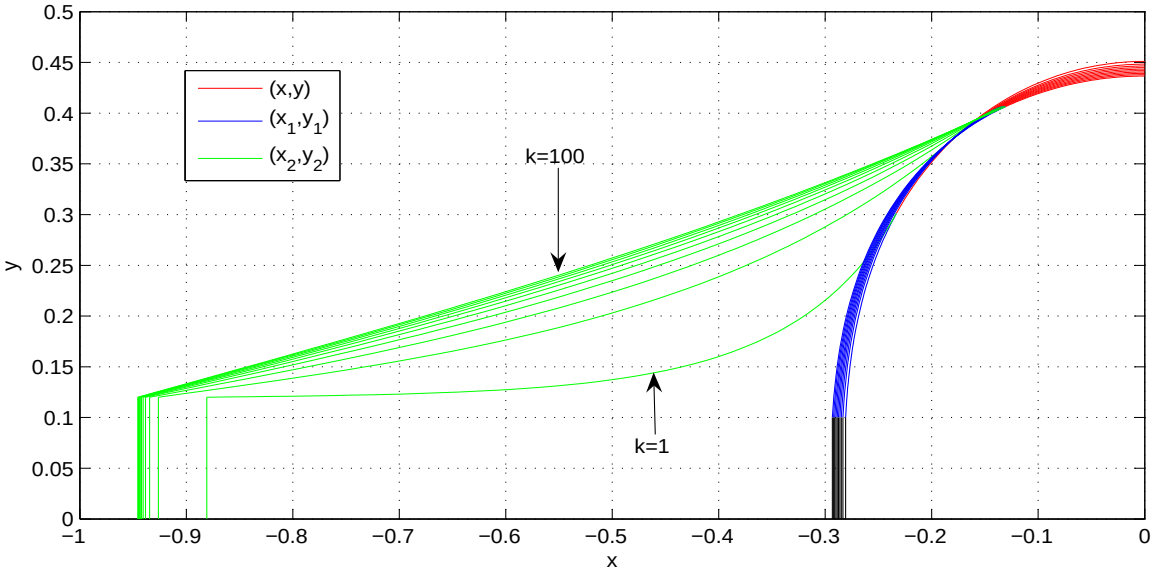

Figure 24: System profiles with $\beta = 1,\ p = 100,\ f_1 = 0$ with $k = 1 \ldots 100$.

The influence of the stiffness k for $f_1 \neq 0$ is left for further investigation. So we keep the value $k = 1$ in the following graphics.

Having in mind that $p = 100$ is obviously a rather high internal pressure making the segment a very tense device we now decrease the pressure by a factor $\frac{1}{10}$ and see what happens. Let us first consider the shape of the system under a pressing force $f_1 = 0.5$ for $\beta = 0$ and $\beta = 1$ (see Figures 25 and 26).

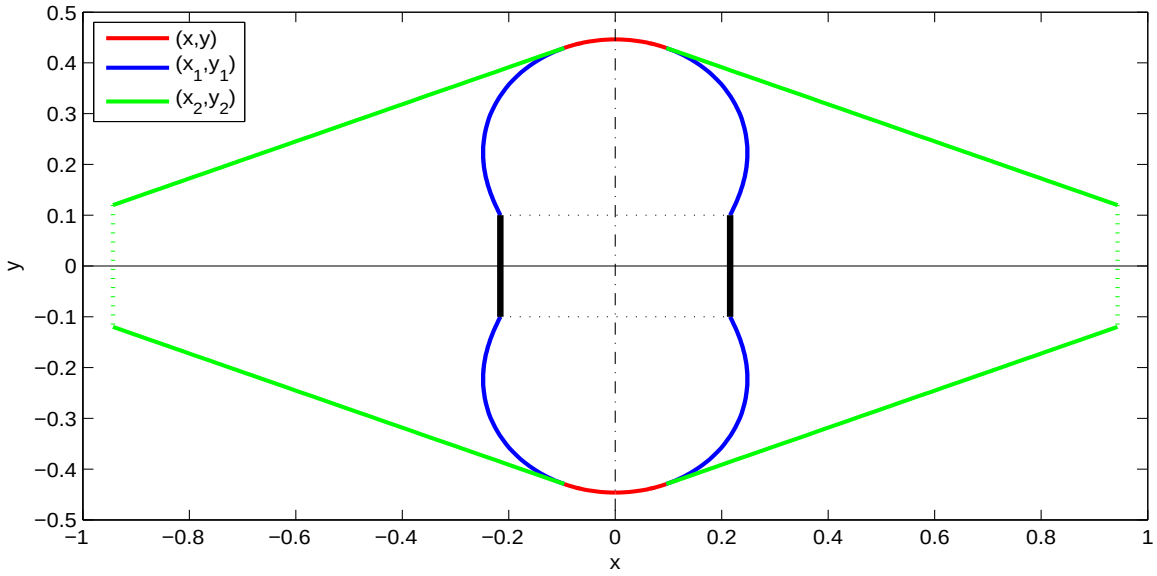

Figure 25: System shape with $\beta = 0$, $p = 10$, $k = 1$, $f_1 = 0.5$.

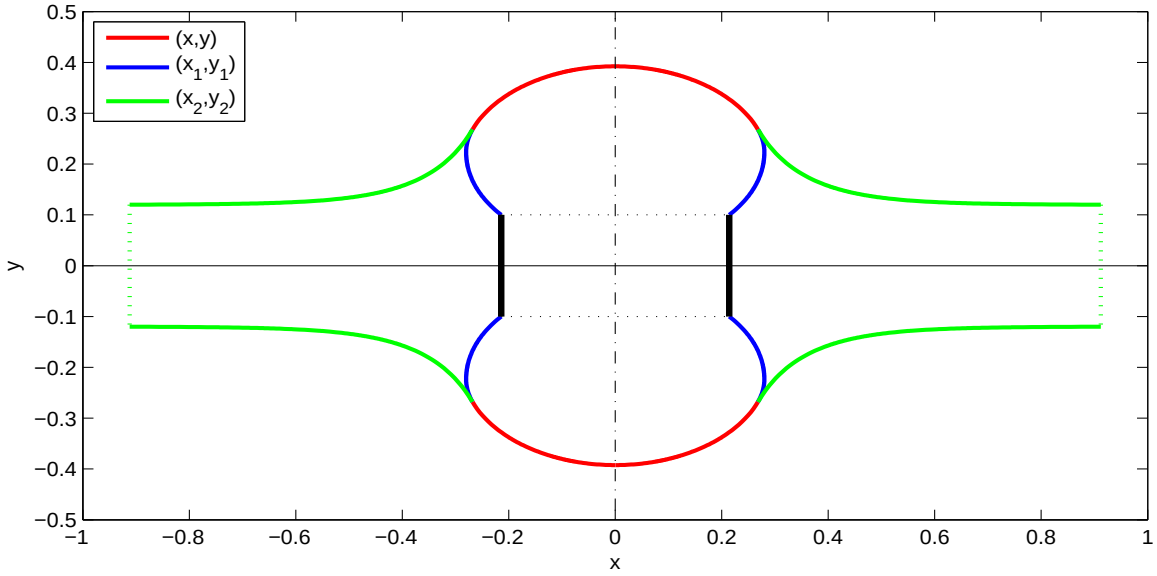

Figure 26: System shape with $\beta = 1$, $p = 10$, $k = 1$, $f_1 = 0.5$.

Mind, on the contrary, that with $p = 100$ the tyre-like shapes just begin to show up at $f_1 = 5$ (see Fig. 18). Finally we sketch a family of shapes for $\beta = 2$ in Figure 27, and we conclude this gallery in showing some characteristics for $p = 10$.

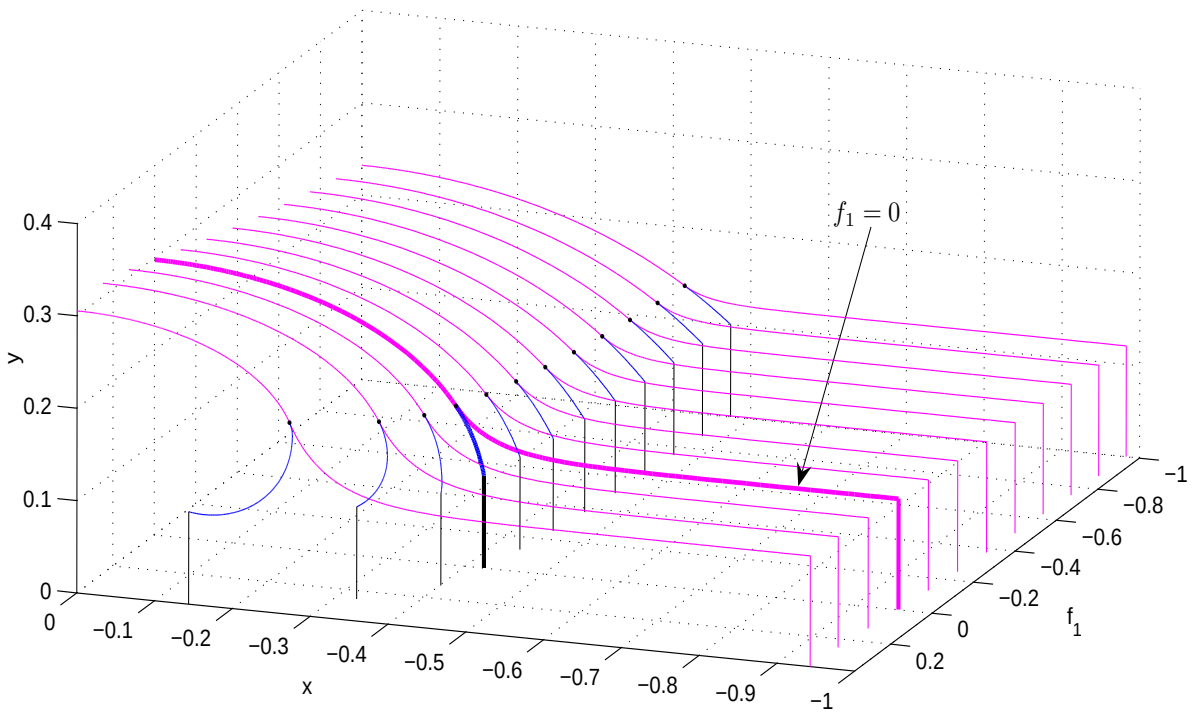

Figure 27: Profiles for $p = 10$, $\beta = 2$, $k = 1$ with $-1 \leq f_1 \leq 0.4$.

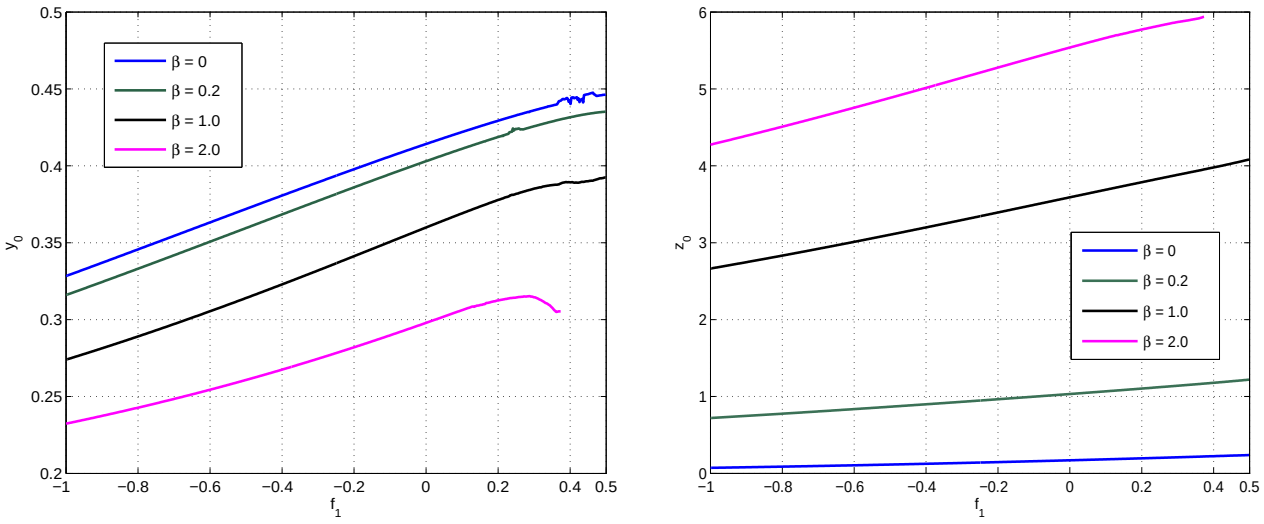

Figure 28: Characteristics for $p = 10$ and various β: y_0 vs. f_1 (left), z_0 vs. f_1 (right).

Remark: Different positive bounds for f_1 and a little trembling in the last characteristics may be due to some numerical difficulties connected with the above mentioned singularity in the differential equations.

5.4 Some 3D-Views

Concluding our gallery of graphics we show some 3D-views of the system *inflated segment/ enveloping vein*, with stiffness $k = 1$ and zero internal force $f_1 = 0$. The following four figures should be compared with Figures 2, 3, 8 to 12.

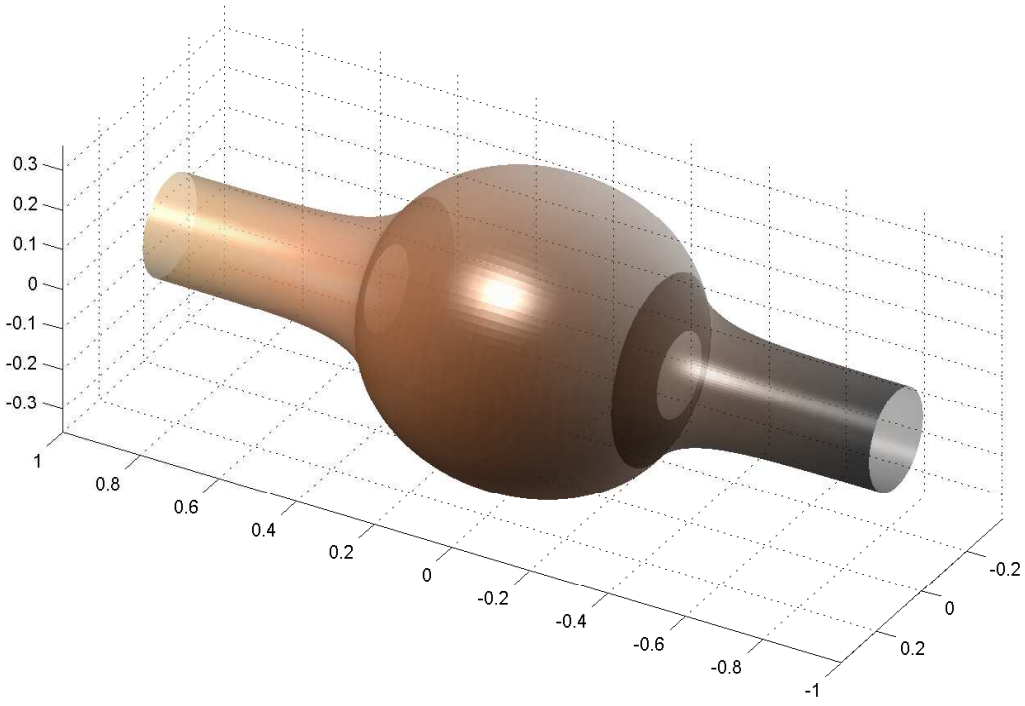

Figure 29: Rotated shape for $\beta = 1, r_2 = 0.12, p = 10$

The latter ones present (each a quarter of) the system shapes for various values of the internal pressure p and vein stiffness β. Figures 29 to 31 show the system under an internal pressure $p = 10$ (medium-sized) with stiffness $\beta = 1$ (medium; equal stiffnesses of segment and vein), $\beta = 0.001$ (very low), and $\beta = 5$ (high), respectively. The effect of 'thin' and 'thick' vein is obvious. Figure 32 finally shows the system with $\beta = 1$ under high inflating pressure $p = 100$, i.e., segment close to its maximum volume state. The corresponding contact pressures z can be found in Figures 14 to 17.

6 Conclusion

In this paper we set up and investigate a mathematical model of a balloon-like mechanical device '*segment*' that is inflated within a (long) cylindrical compliant tube ('*vein*'). Put in concrete terms, compliance means hyperelasticity with a special anisotropy (meridional inextensibility). The background system can be seen as part of a worm crawling in a compliant tube or as a system in medical endoscopy. The investigations continue former work, that concerned freely inflating segments and rigid surrounding tubes, respectively, [7], [8].

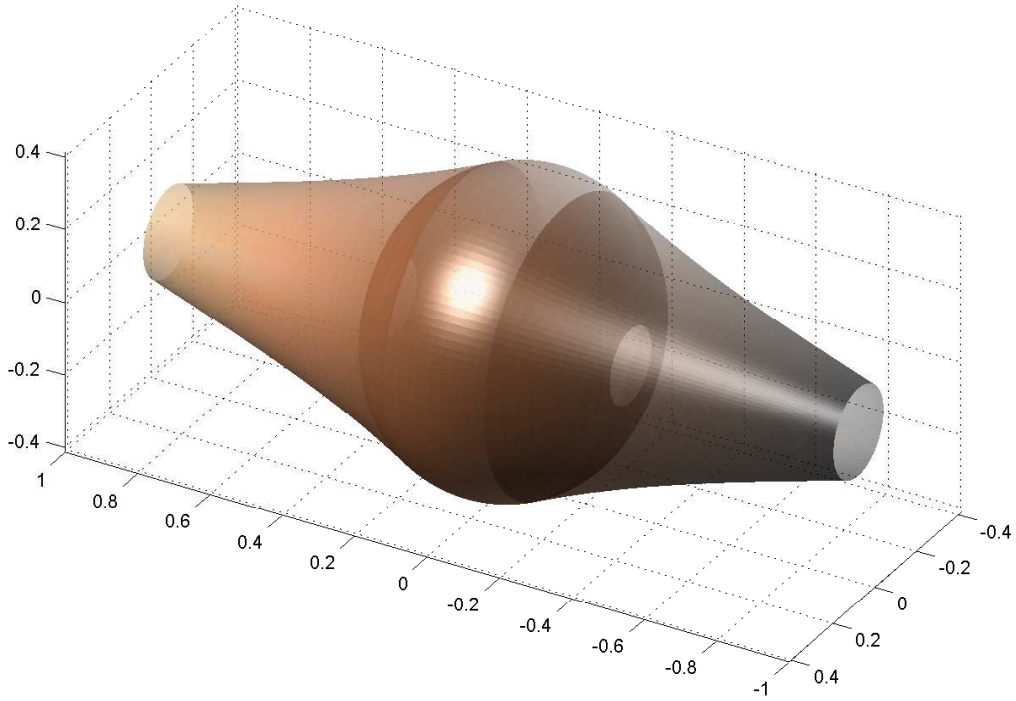

Figure 30: Rotated shape for $\beta = 0.01, r_2 = 0.12, p = 10$

The mathematical basis is taken from [9], where the governing boundary value problem was derived out of the Principle of Minimal Potential Energy formulated as an optimal control problem with state constraint.

The analysis of the optimality condition ends up with a 9-dimensional ordinary boundary value problem where several *given* parameters (the internal pressure of the segment in the first place) and *to-be-matched* parameters enter the differential equations and the boundary conditions as well. All geometrical and physical quantities are appropriately normalized so that the boundary value problem applies to segment-vein systems of arbitrary absolute size and elasticity. A solution of the boundary value problem describes the shape of the deformed system (without using any presupposition about the shape of the deformed system, as done, e.g., in [2] and [6]), afterwards the internal pressure between the contacting segment and vein can be determined utilizing a formula.

Once again we emphasize that the aim of our investigations was to see the *principal behavior* of the modeled system. To this end the presented simulation results were achieved by using choice parameter values which we hoped to be reasonable. Any dissatisfied specialist is invited to do his own simulations using our source code (on request).

Various possible improvements of the presented model are at hand. We list some samples.

Regarding membrane material:

- Drop the Hooke law and switch to some other material constitutions, maybe of Mooney-Rivlin type and different for segment and vein; easily done within the source code by exchanging the ψ-functions with any others.

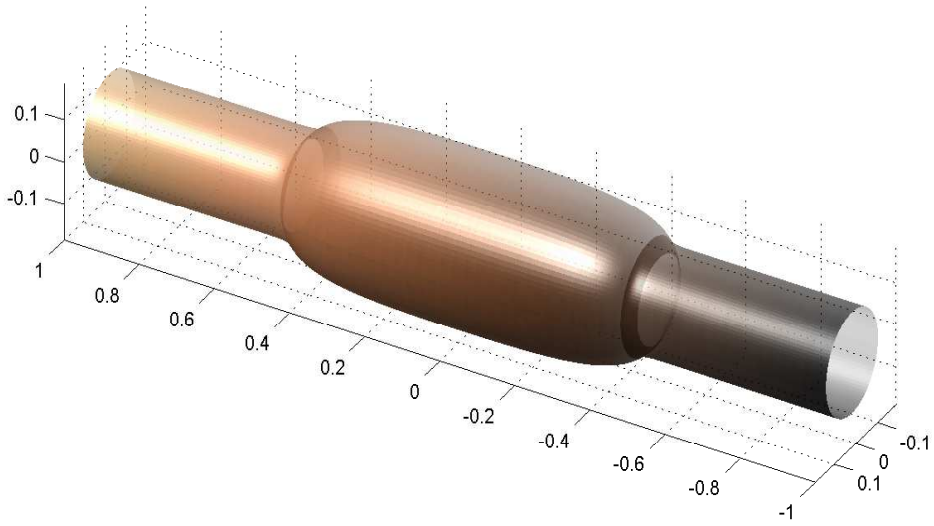

Figure 31: Rotated shape for $\beta = 5, r_2 = 0.12, p = 10$

- Take into consideration finite strength of the membranes: introduce bounds for the stress resultants n^{11} and n^{22} (see [8]) and therefrom find a maximal feasible pressure $p_{\max}$.
- Relax the constraint of meridional inextensibility; this might give a more realistic rheology - but at the expense of losing the (theoretically and computationally valuable) invariance of arc-lengths and the existence of the maximum volume configuration of the inflated ($p = \infty$) segment.

Regarding system geometry:

- Allow for longitudinal asymmetry of the system: eccentric position of the segment within the vein, or different spring stiffnesses. The optimality conditions remain essentially unchanged but, possibly, the analysis cannot be restricted to one quarter of a longitudinal cut anymore.
- Drop the original circular cylindrical shape of the tube: allow for a constriction or for non-constant thickness (Some first investigations of segments eccentrically placed within a rigid stenosis were done in [5]).

Regarding applications:

- Consider two mutually non-compensating forces instead of $\pm f_1$; such forces could be generated by fluid filling within the vein. Possibly, these forces must be equilibrated by tangential forces in the contact area ("friction").

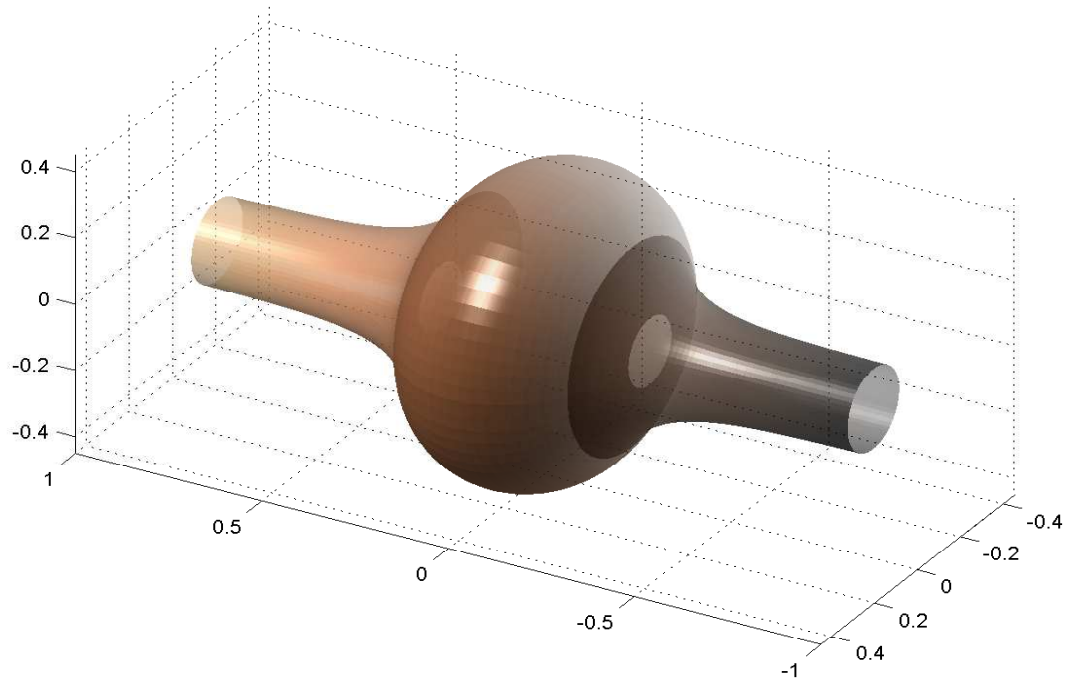

Figure 32: Rotated shape for $\beta = 1, r_2 = 0.12, p = 100$

- Replace the isobaric process *'change of shape by variable f_1 at constant pressure p_0'* by an isochoric one, *'change of shape by variable f_1 at constant volume v_0 of the segment'*. Then the pressure p varies in the neighborhood of the pre-adjusted pressure p_0 (corresponding to v_0), and it is governed by the additional isoperimetric side condition $\int_{-\xi_1}^{\xi_1} y_1^2 dx = v_0$, [7]. This setting could be crucial in the field of worm-like locomotion systems with $\pm f_1$ generated by muscles.

- As to the background application problems it is clear that the presented investigations and simulation results are only a first step towards a description of, e.g., stenosis dilatation. Until now nothing has been done to capture a complicated rheology and rotational non-symmetry (or randomness) of the constricting plaque.

  (One day, during a meeting, a medical colleague was asked how he can hit the right parameter values (e.g., pressure) in trachea dilation. "By intuition" he replied. Maybe, our paper gives some modest hints to strengthen the quantitative bases of this method.)

- And finally, concerning worm-like motion, at least a concatenation of segments within a rigid or compliant surrounding, considering also tangent surface contact forces (driving force or friction), demands an intensified theoretical attention.

Acknowledgement. The authors thank Prof. Klaus Zimmermann, head of the department for Technical Mechanics at TU Ilmenau, for his steady interest and support. We appreciate the interested collaboration of his student Simon Hergenroeder in our investigations. And we remind Harald Abeszer for his essential contributions in optimal control.

References

[1] Ascher, U.M.; Mattheji, R.M.; Russell, R.D.: Numerical Solution of Boundary Value Problems for Ordinary Differential Equations. SIAM, Philadelphia, 1995.

[2] Boegelsack, G.: On fluidmechanical compliant actuators. 19th Working Meeting of IFToMM Commission A, Kaunas, 2000, 51-56.

[3] Green, A.; Zerna, W.: Theoretical Elasticity, Clarendon Press, Oxford, 1954.

[4] Hoffmann, A.; Marx, B.; Vogt, W.: Mathematik für Ingenieure - Theorie und Numerik, Band 2. Pearson Studium, München, 2006.

[5] Koch, H.: Inflationsprozesse in festen Röhren als Optimalsteuerproblem. Diplomarbeit, Fakultät Math. Nat., TU Ilmenau, 2009.

[6] Shinohara, H., et al.: Derivation of a mathematical model for pneumatic artificial muscles. 4th IFAC Sympos. on Mechatronic Systems, Heidelberg (Germany), 2006, 266-270.

[7] Steigenberger, J.: Contribution to the mechanics of worm-like motion systems and artificial muscles. Biomech. Model. Mechanobiol. **2**, 2003, 37-57.
(DOI 10.1007/s10237-003-0027-2).

[8] Steigenberger, J.; Abeszer, H.: Quasistatic inflation processes within rigid tubes.
- ZAMM **88**, No.7, 2008, 556-572. (DOI 10.1002/zamm.200700166).
- TU Ilmenau (Germany), Inst.Math., Preprint No. M09/06, 2006,
(http://www.tu-ilmenau.de/fakmn/Preprints.528.0.html).

[9] Steigenberger, J.; Abeszer, H.: Quasistatic inflation processes within compliant tubes, Part1: Analytical investigations. TU Ilmenau (Germany), Inst.Math., Preprint No. M29/09, 2009. (http://www.tu-ilmenau.de/fakmn/Preprints.528.0.html).

[10] Steigenberger, J.; Behn, C.: Worm-like Locomotion Systems. Oldenbourg Verlag, Muenchen, 2012, 195 pp.

[11] Venhaus, M.: Ein Beitrag zur Modellbildung und Simulation der Ballondilatation von Atemwegstenosen. Dissertation, Fakultät Maschinenbau, TU Ilmenau, 2006.

Authors

Werner Vogt, Priv.-Doz. i.R.
Technische Universität Ilmenau, Institut für Mathematik
98684 Ilmenau, Deutschland

Joachim Steigenberger, Univ.-Prof. i.R.
Technische Universität Ilmenau, Institut für Mathematik
98684 Ilmenau, Deutschland

Peter Maißer, Prof. i.R.
Institut für Mechatronik e.V.
09126 Chemnitz, Deutschland